Research Article

Essaid Aourir, H. Laeli Dastjerdi, Mustapha Oudani, Kamal Shah and Thabet Abdeljawad*

On the existence and the approximation of solutions of linear and nonlinear fractional order delay-integro-differential equations with vanishing variable delays

https://doi.org/10.1515/nleng-2025-0192
Received March 26, 2025; accepted December 1, 2025;
published online April 7, 2026

Abstract: In this study, we investigate the application of the meshless collocation technique using radial basis functions (RBF) to approximate a class of linear and nonlinear fractional order delay-integro-differential equations with vanishing variable delays. Such equations, formulated within the framework of fractional calculus, are particularly useful for modeling processes with memory and hereditary characteristics, providing a more accurate representation of many physical and engineering phenomena than classical integer-order models. First, we prove the existence and uniqueness of solutions of the studied equation for both linear and nonlinear cases. Then, we develop an RBF interpolation combined with the Gauss–Legendre quadrature formula, enabling the proposed approach to solve the equations without relying on background approximation cells. The developed method is computationally efficient, stable, and requires low memory. Furthermore, the error analysis of this scheme is discussed. Several computational tests are presented to demonstrate the reliability and precision of the proposed technique for solving the considered equations. The obtained results are compared with analytical solutions, the moving least squares method, and other existing approaches to confirm the effectiveness and applicability of the proposed scheme.

Keywords: caputo derivative; fractional pantograph delay integro-differential equations; vanishing variable delays; collocation method

MSC 2020: 45D05; 34A08; 26A33; 45J05; 65L20

1 Introduction

Fractional calculus has attracted the scientific community's attention as a robust mathematical framework for extending the concepts of differentiation and integration to non-integer orders. While classical calculus is limited to integer-order operations, fractional calculus provides a more generalized approach [1, 2]. Furthermore, it allows for the incorporation of memory effects and hereditary properties. It is worth noting that this characteristic is particularly important when modeling real-world phenomena. Moreover, one intrinsic feature of fractional calculus, not given by classical calculus, is its ability to model the dynamic nature of systems. Researchers utilized this property to formulate several problems from various fields, including fluid mechanics, control theory, materials science, and signal processing. Additionally, fractional calculus is used in biology [3, 4], complex physics system and finance. More specifically, differential equations (DEs) and Volterra integral equations (VIEs) with non-integer order derivatives were used to simulate several real-world phenomena, such as continuum mechanics, fluid-dynamics traffic model [5], chemistry, and

*Corresponding author: Thabet Abdeljawad, Department of Mathematics and Sciences, Prince Sultan University, Riyadh 11586, Saudi Arabia; Department of Fundamental Sciences, Faculty of Engineering and Architecture, Istanbul Gelisim University, Avcilar, 34310, Istanbul, Türkiye; and Department of Mathematics and Applied Mathematics School of Science and Technology, Sefako Makgatho Health Sciences University, Ga-Rankuwa, South Africa, E-mail: tabdeljawad@psu.edu.sa
Essaid Aourir, Laboratory of Mathematical Engineering and Computer Science, Faculty of Science, Ibn Zohr University, Agadir, Morocco, E-mail: essaid.aourir@edu.uiz.ac.ma
H. Laeli Dastjerdi, Department of Mathematics Education, Farhangian University, P. O. Box 14665-889, Tehran, Iran, E-mail: h.laeli@cfu.ac.ir
Mustapha Oudani, TICLab Laboratory, College of Engineering & Architecture, International University of Rabat, Rabat 11103, Morocco, E-mail: mustapha.oudani@uir.ac.ma
Kamal Shah, Department of Mathematics and Sciences, Prince Sultan University, Riyadh 11586, Saudi Arabia, E-mail: kshah@psu.edu.sa

Open Access. © 2026 the author(s), published by De Gruyter. This work is licensed under the Creative Commons Attribution 4.0 International License.

acoustics [6]. For a detailed review, the reader is invited to see [7, 8].

Among well-studied fractional DEs are pantograph differential equations (PDEs). The pantograph DEs were initially used for scaling and drawing. Currently, it is used in modern models for electric trains, material and laser modeling. Pantograph equations are a class of integro-differential equations (IDEs) with proportional delays. These kinds of equations appear in several scientific and applied fields, such as biology, control theory, astrophysics, economics, and electrodynamics [9]. Notably, an important question on mathematical research is the investigation of fractional delay-integro-differential equations (FDIDEs). These equations arise from several scientific and engineering problems due to their ability to model complex dynamical systems that incorporate memory effects and hereditary properties. However, their complex structure poses multiple difficulties when seeking explicit analytical solutions. In fact, finding analytical solutions for such equations is always a hard task. Instead, one may use numerical techniques. Actually, several stable numerical methods were proposed for FDIDEs. In this work, we use a collocation method based on radial basis functions (RBF) to derive an approximate solution for both linear and nonlinear FDIDEs characterized by vanishing variable delays. The general formulation of these equations is given as follows:

$$\begin{cases} D^{\alpha}u(t) = a_1(t)u(t) + a_2(t)u(\theta(t)) + a_3(t)\displaystyle\int_0^t K_1(t,s)u(s)\mathrm{d}s \\ \quad + a_4(t)\displaystyle\int_0^{\theta(t)} K_2(t,\tau)u(\tau)\mathrm{d}\tau + f(t), \\ u(0) = \lambda, \text{ where } \lambda \text{ is an arbitrary real constant,} \end{cases} \tag{1}$$

and

$$\begin{cases} D^{\alpha}u(t) = a_1(t)u(t) + a_2(t)u(\theta(t)) + a_3(t)\displaystyle\int_0^t K_1(t,s)G_1(u(s))\mathrm{d}s \\ \quad + a_4(t)\displaystyle\int_0^{\theta(t)} K_2(t,\tau)G_2(u(\tau))\mathrm{d}\tau + g(t), \\ u(0) = \lambda, \text{ where } \lambda \text{ is an arbitrary real constant,} \end{cases} \tag{2}$$

in which $t \in I := [0,T]$, $\alpha \in (0,1]$, D^{α} is expressed in Caputo sense and designates the fractional derivative of fractional order α, $G_i \in C^1(\mathbb{R})$ (i = 1, 2), while $a_j(t)$ (j $= 1, 2, \ldots, 4$), $g(t)$ and $f(t)$ are given bounded functions, $f: [0,\infty) \to (\infty,\infty)$, $g: [0,\infty) \to (\infty,\infty)$, The delay function $\theta(t)$ is expressed as $\theta(t) := t - \kappa(t)$ and adheres to the following conditions, as stated in [10]:

(C1) At $t = 0$, the function $\kappa(t)$ satisfies $\kappa(0) = 0$, while for all $t \in (0,T]$, it remains strictly positive, ensuring a vanishing delay.

(C2) $\exists \upsilon \in (0,1)$ where $\theta(t)$ is bounded by $\theta(t) \leq \upsilon t$ for all $t \in I$. Moreover, the derivative condition $\theta'(t) \geq \upsilon_0 > 0$ holds.

(C3) The function $\theta(t)$ belongs to the class of continuously differentiable functions, i.e., $\theta(t) \in C^1(I)$.

Furthermore, $K_i \in C(D_i)$ in which $i = 1, 2$, $D_1 := \{(t,s): 0 \leq s \leq t \leq T\}$, and $D_2 := \{(t,\tau): 0 \leq \tau \leq \theta(t) \leq \theta(T)\}$. A notable case covered by Equation (1) is when the delay function takes the form $\theta(t) = \upsilon t$, indicating a proportional delay where υ lies within the range (0,1).

The linear case, $\theta(t) = \upsilon t = t - (1-\upsilon)t =: t - \kappa(t) (0 < \upsilon < 1)$ (proportional delay) is also called the pantograph delay function. In this investigation, we are considering a vanishing delay, although the proposed methods may also be employed with nonvanishing delay too. When $\theta(t) = \upsilon t$, called the pantograph, numerous schemes were suggested to approximate (1). A numerical algorithm is offered for solving the equations (1) and (2) in which $\theta(t)$ is more general than pantograph.

Consider $\Gamma(\cdot)$ as the Gamma function. Given $n \in \mathbb{N}$ and $\alpha \in \mathbb{R}$ where $n-1 < \alpha < n$, then the derivative according to Caputo is given by the following formula:

$$D^{\alpha}u(t) = \frac{1}{\Gamma(n-\alpha)}\int_0^t \frac{u^{(n)}(s)}{(t-s)^{(\alpha-n+1)}}\mathrm{d}s, \quad t \in [0,T].$$

Researchers have recently turned their attention to FDIDEs. In [11], numerical procedure using Euler wavelets has been proposed for FDIDEs. A numerical method using Haar wavelet for solving these equations has been used in [12]. In [13], Yang and Huang employed a spectral collocation approach for FDIDEs.

Meshless techniques have emerged as a widely adopted approach for scattered data estimation, providing function approximations without the necessity of mesh generation within the domain. These methods are regarded as highly efficient and powerful computational tools across various fields. Commonly employed mesh-free schemes in scientific research can be broadly categorized into moving least squares (MLS) and RBFs methods. One of the most notable advantages of numerical techniques based on RBFs is their independence from meshing. In many RBF-based approaches, the solution's accuracy and stability are greatly affected by an essential positive factor called the shape parameter. A substantial body of research has been dedicated to determining the optimal value of this shape parameter, a task that proves to be quite challenging in most

cases. Over the years, RBF-based methods have been extensively investigated to deal with different types of PDEs. This methodology has been successfully extended to numerous applications, as illustrated in [14].

A considerable number of publications have introduced numerical methods for solving various sorts of problems using mesh-free methods, such as VIEs and integro-differential equations [15–19]. RBF is a highly advanced meshless approach that have been successfully employed and developed for several different applications in recent years. The advantages of this approach include simplicity of implementation and the ability to achieve high convergence by utilizing infinitely differentiable RBFs.

The following are the benefits of the suggested technique:

- The approach is independent of the domain's geometry, making it suitable for different problems.
- This methodology can be generalized to address other types of fractional differential-integral equations (FDIDEs).
- Distinguished by its high accuracy, this method eliminates the need for meshing, accommodates complex and irregular geometric domains, and remains unaffected by the problem's dimensionality.
- From a computational standpoint, the implementation of this technique is straightforward.

The subsequent sections are as follows:

- In Section 2, we recall key principles of fractional calculus, establishing the groundwork for the subsequent discussions.
- In Section 3, we establish, for both the linear and the nonlinear case, the structural results of solutions (existence and uniqueness).
- Section 4 presents a detailed overview of radial basis function (RBF) approximations, highlighting essential properties and expressions.
- In Section 5, we propose a numerical technique based on RBFs to tackle (1) and (2).
- we study, in the Section 6, the convergence behavior of the proposed method, ensuring its mathematical soundness.
- Section 7 illustrates the accuracy and effectiveness of our approach by comparing numerical results for equations (1) and (2) with existing methodologies.
- Finally, Section 8 summarizes the findings and the limitations of the developed method and presents some ideas for future research.

2 Preliminaries

The upcoming section explores the foundational concepts of fractional calculus, outlining its main principles, fundamental properties, and most used definitions that distinguish it from classical calculus [20].

Definition 2.1. Let $h\colon \mathbb{R}^+ \to \mathbb{R}$. The function $h \in C_\mu[0,\infty)$, and $\mu \in \mathbb{R}$, if $\exists p$ such that $p > \mu$ and $h(t) = t^p h_1(t)$, where $h_1(t) \in C[0,\infty)$.

Furthermore, the function h is considered to be in the space $C_\mu^n[0,\infty)$ if its n-th derivative satisfies $h^{(n)}(t) \in C_\mu[0,\infty)$ for some $n \in \mathbb{N}$. Several definitions exist for fractional derivatives, among which the most frequently utilized ones include those of Riemann-Liouville, Grünwald-Letnikov, and Caputo.

Definition 2.2. For a function $h \in C_\mu$, the given equation

$$J^\alpha h(t) = \frac{1}{\Gamma(\alpha)} \int_a^t (t-s)^{\alpha-1} h(s)\,\mathrm{d}s, \quad \alpha > 0, \quad t > a, \tag{3}$$

defines the Riemann-Liouville fractional integral operator of order $\alpha \geq 0$. Here, $\Gamma(\alpha)$ is the gamma function, defined as

$$\Gamma(\alpha) = \int_0^\infty t^{\alpha-1} e^{-t}\,\mathrm{d}t. \tag{4}$$

By convention, for $\alpha = 0$, the operator reduces to the identity function:

$$J^0 h(t) = h(t). \tag{5}$$

Clearly, for $\beta_1, \beta_2 \in \mathbb{R}$, we have

$$J^\alpha\big(\beta_1 f(t) + \beta_2 g(t)\big) = \beta_1 J^\alpha f(t) + \beta_2 J^\alpha g(t).$$

Definition 2.3. For a function $h(t)$, the following equation:

$$D^{\alpha}h(t) = \begin{cases} \dfrac{1}{\Gamma(n-\alpha)}\displaystyle\int_0^t (t-s)^{n-\alpha-1}h^{(n)}(s)\,\mathrm{d}s, & \text{if } n-1<\alpha\le n, \quad n\in\mathbb{N}, \\ \dfrac{\mathrm{d}^n h(t)}{\mathrm{d}t^n}, & \text{if } \alpha = n. \end{cases} \tag{6}$$

defines the Caputo fractional derivative of order $\alpha > 0$. The parameter $\Gamma(\cdot)$ represents the gamma function, which is used for normalization. This formulation is widely employed in fractional calculus as it allows for initial conditions to be expressed in terms of classical derivatives, making it particularly useful in physical and engineering applications.

For $t > 0, h \in C_{\mu}^{n}, \alpha \ge -1$, integral operators of Riemann and Caputo fulfill:

$$D^{\alpha}J^{\alpha}h(t) = h(t),$$

and

$$J^{\alpha}D^{\alpha}h(t) = h(t) - \sum_{k=0}^{m-1}\frac{h^{(k)}(0^{+})}{k!}t^{k},$$

$$m-1<\alpha\le m.$$

Definition 2.4. The set of functions whose derivative is absolutely continuous $(n-1)$-st is noted $\mathcal{A}^n[a,b]$. Indeed, the function $h(t)$ is in $\mathcal{A}^n[a,b]$ for that there is a function $\upsilon(t) \in L^1[a,b]$ such that

$$h^{(n-1)}(t) = h^{(n-1)}(0) + \int_a^t \upsilon(\tau)\mathrm{d}\tau.$$

We have for $\alpha > 0$ for a function $h \in \mathcal{A}^n[a,b]$, the Riemann fractional derivative is generally expressed as follows:

$$D^{\alpha}h(t) = \left(\frac{\mathrm{d}}{\mathrm{d}t}\right)^{n} J^{n-\alpha}h(t), \quad n-1<\alpha\le n.$$

Lemma 1. *Let $\alpha > 0, n = [\alpha]$ and $h(t) = t^c$ for some $c \ge 0$. Then,*

$$D^{\alpha}h(t) = \begin{cases} 0 & \text{if } c\in\{0,1,\dots,n-1\} \\ \dfrac{\Gamma(c+1)}{\Gamma(c+1-\alpha)}t^{c-\alpha} & \text{if } c\in N \text{ and } c\ge n \text{ or } c \text{ not in } N \text{ and } c>n-1. \end{cases}$$

3 Existence and uniqueness of solutions

3.1 Linear case

Theorem 3.1 (Existence and Uniqueness for the Linear Equation). *Assume that*

- *The functions $a_j(t)$ $(j = 1,2,3,4)$, the inhomogeneity $f(t)$, and the kernels $K_i(t,s)$ $(i = 1,2)$ are continuous and bounded on the interval $I = [0,T]$.*
- *The delay function $\theta(t) = t - \kappa(t)$ satisfies:*
  - (C1) *$\kappa(0) = 0$ and $\kappa(t) > 0$ for $t \in (0,T]$ (i.e. the delay vanishes at $t = 0$);*
  - (C2) *$\theta(t) \le \upsilon t$ for some $\upsilon \in (0,1)$ and all $t \in I$, with $\theta'(t) \ge \upsilon_0 > 0$;*
  - (C3) *$\theta(t) \in C^1(I)$.*
- *There exists a constant*

$$L := \frac{T^{\alpha}}{\Gamma(\alpha+1)}\left(\sup_{t\in I}|a_1(t)| + \sup_{t\in I}|a_2(t)| + \sup_{t\in I}|a_3(t)|\,M_{K_1} + \sup_{t\in I}|a_4(t)|\,M_{K_2}\right) < 1,$$

where M_{K_1} and M_{K_2} are appropriate bounds for the integral operators induced by K_1 and K_2.

Then the linear fractional integro-differential equation

$$\begin{cases} D^{\alpha}u(t) = a_1(t)u(t) + a_2(t)u(\theta(t)) + a_3(t)\displaystyle\int_0^t K_1(t,s)u(s)\,\mathrm{d}s \\ \quad + a_4(t)\displaystyle\int_0^{\theta(t)} K_2(t,\tau)u(\tau)\,d\tau + f(t), \\ u(0) = \lambda, \end{cases} \tag{7}$$

admits a unique solution in the Banach space $C([0,T],\mathbb{R})$.

Proof. We first recall that, for a real order $\alpha \in (0,1]$, the caputo-derivative is

$$D^{\alpha}u(t) = \frac{1}{\Gamma(1-\alpha)}\int_0^t \frac{u'(s)}{(t-s)^{\alpha}}\,\mathrm{d}s,$$

and its associated fractional integral operator is given by

$$(I^{\alpha}\varphi)(t) = \frac{1}{\Gamma(\alpha)}\int_0^t (t-s)^{\alpha-1}\varphi(s)\,\mathrm{d}s.$$

Applying I^{α} to both sides of (7) and using the initial condition $u(0) = \lambda$, one obtains the equivalent integral equation:

$$\begin{aligned} u(t) = \lambda + \frac{1}{\Gamma(\alpha)}\int_0^t (t-s)^{\alpha-1}\Big\{ & a_1(s)u(s) + a_2(s)u(\theta(s)) \\ & + a_3(s)\int_0^s K_1(s,\xi)u(\xi)\,\mathrm{d}\xi \\ & + a_4(s)\int_0^{\theta(s)} K_2(s,\tau)u(\tau)\,\mathrm{d}\tau \\ & + f(s)\Big\}\,\mathrm{d}s. \end{aligned} \tag{8}$$

Define the operator

$$\Phi : C([0,T],\mathbb{R}) \to C([0,T],\mathbb{R})$$

defined by

$$\begin{aligned} (\Phi u)(t) = \lambda + \frac{1}{\Gamma(\alpha)}\int_0^t (t-s)^{\alpha-1}\Big\{ & a_1(s)u(s) + a_2(s)u(\theta(s)) \\ & + a_3(s)\int_0^s K_1(s,\xi)u(\xi)\,\mathrm{d}\xi \\ & + a_4(s)\int_0^{\theta(s)} K_2(s,\tau)u(\tau)\,\mathrm{d}\tau \\ & + f(s)\Big\}\,\mathrm{d}s. \end{aligned} \tag{9}$$

Using the boundedness of a_j, K_i, and the properties of $\theta(t)$, one can show that $\forall u, v \in C([0,T],\mathbb{R})$,

$$\begin{aligned} \|\Phi u - \Phi v\| \le \frac{T^{\alpha}}{\Gamma(\alpha+1)}\Big(& \sup_{t\in I}|a_1(t)| + \sup_{t\in I}|a_2(t)| \\ & + \sup_{t\in I}|a_3(t)|\,M_{K_1} + \sup_{t\in I}|a_4(t)|\,M_{K_2}\Big) \\ & \times \|u - v\|. \end{aligned}$$

Because the constant on the right-hand side is less than 1 by hypothesis, Φ is a contraction. Next, using the contraction principle, $\exists! u \in C([0,T],\mathbb{R})$ where $\Phi u = u$, which is equivalent to the unique solution of (7). □

3.2 Nonlinear case

Theorem 3.2 (Existence and Uniqueness for the Nonlinear Equation). *Assume that*

- *The functions $a_j(t)$ $(j = 1,2,3,4)$, the inhomogeneity $g(t)$, and the kernels $K_i(t,s)$ $(i = 1,2)$ are continuous and bounded on the interval $I = [0,T]$.*
- *The delay function $\theta(t) = t - \kappa(t)$ satisfies:*
  - (C1) *$\kappa(0) = 0$ and $\kappa(t) > 0$ for $t \in (0,T]$;*
  - (C2) *$\theta(t) \le \upsilon t$ for some $\upsilon \in (0,1)$ and all $t \in I$, with $\theta'(t) \ge \upsilon_0 > 0$;*
  - (C3) *$\theta(t) \in C^1(I)$.*
- *The functions $G_i \in C^1(\mathbb{R})$ (for $i = 1,2$) are Lipschitz continuous with Lipschitz constants L_{G_i}.*
- *There exists a constant*

$$\begin{aligned} L := \frac{T^{\alpha}}{\Gamma(\alpha+1)}\Big(& \sup_{t\in I}|a_1(t)| + \sup_{t\in I}|a_2(t)| \\ & + \sup_{t\in I}|a_3(t)|\,\widetilde{M}_{K_1} + \sup_{t\in I}|a_4(t)|\,\widetilde{M}_{K_2}\Big) < 1, \end{aligned}$$

where $\widetilde{M}_{K_1}$ and $\widetilde{M}_{K_2}$ denote appropriate bounds for the integral operators induced by K_1 and K_2 that incorporate the Lipschitz constants of G_1 and G_2.

Then the nonlinear FIDE

$$\begin{cases} D^{\alpha}u(t) = a_1(t)u(t) + a_2(t)u(\theta(t)) + a_3(t)\displaystyle\int_0^t K_1(t,s)G_1(u(s))\,\mathrm{d}s \\ \quad + a_4(t)\displaystyle\int_0^{\theta(t)} K_2(t,\tau)G_2(u(\tau))\,\mathrm{d}\tau + g(t), \\ u(0) = \lambda, \end{cases} \tag{10}$$

have a single solution in $C([0,T],\mathbb{R})$.

Proof. Proceeding as in the linear case, we integrate (10) using the operator I^{α}. In fact, with the Caputo derivative and $u(0) = \lambda$, we obtain the equivalent integral equation:

$$\begin{aligned} u(t) = \lambda + \frac{1}{\Gamma(\alpha)}\int_0^t (t-s)^{\alpha-1}\Big\{ & a_1(s)u(s) + a_2(s) \\ & \times u(\theta(s)) + a_3(s)\int_0^s K_1(s,\xi)G_1(u(\xi))\,\mathrm{d}\xi \end{aligned}$$

$$+ a_4(s)\int_0^{\theta(s)} K_2(s,\tau)G_2(u(\tau))\,\mathrm{d}\tau + g(s)\Bigg\}\mathrm{d}s.$$

Define the operator $\Psi : C([0,T],\mathbb{R}) \to C([0,T],\mathbb{R})$ by

$$(\Psi u)(t) = \lambda + \frac{1}{\Gamma(\alpha)}\int_0^t (t-s)^{\alpha-1}\Bigg\{a_1(s)u(s) + a_2(s)u(\theta(s)) + a_3(s)\int_0^s K_1(s,\xi)G_1(u(\xi))\,\mathrm{d}\xi + a_4(s)\int_0^{\theta(s)} K_2(s,\tau)G_2(u(\tau))\,\mathrm{d}\tau + g(s)\Bigg\}\mathrm{d}s.$$

Owing to the boundedness of a_j, K_i, the properties of $\theta(t)$, and the Lipschitz continuity of G_i, one can show that for any $u, v \in C([0,T],\mathbb{R})$,

$$\|\Psi u - \Psi v\| \le \frac{T^\alpha}{\Gamma(\alpha+1)}\left(\sup_{t\in I}|a_1(t)| + \sup_{t\in I}|a_2(t)| + \sup_{t\in I}|a_3(t)|\,\widetilde{M}_{K_1} + \sup_{t\in I}|a_4(t)|\,\widetilde{M}_{K_2}\right) \times \|u - v\|.$$

By hypothesis, the constant on the right-hand side is less than 1, so that Ψ is a contraction. Hence, using the contraction principle, $\exists u \in C([0,T],\mathbb{R})$ such that $\Psi u = u$, which is the unique solution of (10). □

4 An outline of RBFs

Over the last decade, considerable developments have been made in the application of RBFs to the numerical solution of various types of problems. Estimating unknown functions over scattered points using RBFs is a highly efficient technique. This technique was not generally applied by developers until Franke [21] published a review article on the evaluation of two-dimensional interpolation approaches. The development of these techniques began with Hardy [22] in 1971 as a multidimensional scattered interpolation approach. Radial basis functions have become popular in interpolation techniques because of their ability to solve problems that are not possible with standard methods. The development of novel basis functions and hybrid approaches has further expanded the scope of RBF applications. In addition, with ongoing research, RBF techniques continue to be refined and extended to address new challenges in scientific computing. As computational power increases, these methods are expected to play an even greater role in tackling large-scale problems that require robust and efficient numerical solutions. Here, RBFs are presented and used to interpolate a function.

Definition 4.1 ([23, 24]). A function $\Phi : \mathbb{R}^d \to \mathbb{R}$ is termed a radial function if it can be expressed in terms of a single variable function $\phi : [0,\infty) \to \mathbb{R}$, satisfying

$$\Phi(t) = \phi\big(\|t\|_2\big).$$

Let $\mathcal{X} = \{t_1, \dots, t_n\} \in \Omega \subset \mathbb{R}^d$ be a chosen set of nodes. In order to obtain an estimate of a function $u(t)$ via a radial function, the following linear combination may be employed

$$u(t) \approx \mathcal{P}_n u(t) = \sum_{k=1}^n d_k \phi\big(\|t - t_k\|\big) + \sum_{r=1}^M b_r p_r(t), \quad t \in \Omega, \tag{11}$$

where $p_1, \dots, p_M$ form a basis for the $M = \binom{d+m-1}{m-1}$ dimensional linear space Π_{m-1}^d of polynomials of total degree less than or equal to $m-1$ in d variables. The interpolation problem is to find $d_k, k = 1, \dots, n$ and $b_r, r = 1, \dots, M$, so that $\mathcal{P}_n u$ across all data fulfills

$$\mathcal{P}_n u(t_i) = u(t_i) = u_i, \quad i = 1, \dots, n., \quad \text{and}$$

$$\sum_{i=1}^n d_i p_j(t_i) = 0, j = 1, \dots, M.$$

This system may be conveniently represented in matrix form as shown below:

$$\begin{pmatrix} \mathcal{J} & \mathbf{p} \\ \mathbf{p}^T & 0 \end{pmatrix}\begin{pmatrix} \mathbf{d} \\ \mathbf{b} \end{pmatrix} = \begin{pmatrix} \mathcal{V} \\ 0 \end{pmatrix}, \tag{12}$$

wherein $\mathcal{J}$ and $\mathbf{p}$ are the $n \times n$ and $n \times M$ matrices with the elements $\mathcal{J}_{ij} = \phi\Big(\Big\|t_i - t_j\Big\|\Big), i, j = 1, \dots, n$ and $\mathbf{p}_{ij} = p_j(t_i), i = 1, \dots, n, j = 1, \dots, M$, respectively. Moreover $\mathbf{d} = \big[d_1, \dots, d_n\big]^T, \mathbf{b} = \big[b_1, \dots, b_N\big]^T$ and $\mathcal{V} = \big[u(t_1), \dots, u(t_n)\big]^T$.

In order to guarantee the well-posed of this interpolation problem, at first, we present some definitions from [24].

Definition 4.2 ([24]). A real-valued continuous even function Φ is called conditionally positive definite of order m on $\mathbb{R}^d$ if

$$\sum_{j=1}^n \sum_{k=1}^n d_j d_k \Phi(t_j - t_k) \ge 0, \tag{13}$$

for any n points $t_1, \dots, t_n \in \mathbb{R}^d$, and $\mathbf{d} = \left[d_1, \dots, d_n\right]^T \in \mathbb{R}^n$ satisfying

$$\sum_{j=1}^{n} d_j t_j^{\alpha} = 0, \quad |\alpha| < m, \quad \alpha \in \mathbb{N}_0^S.$$

The function Φ is called strictly conditionally positive definite of order m on $\mathbb{R}^d$ if the points $t_1, \dots, t_n \in \mathbb{R}^d$ are distinct, and $\mathbf{d} \neq 0$ implies strict inequality in (13).

Remark 4.3. An immediate observation is that a function which is conditionally positive definite of order m on $\mathbb{R}^d$ also is conditionally positive definite of any higher order. The case $m = 0$, i.e., (strictly) conditionally positive definite functions of order zero, yields a class of functions named (strictly) positive definite.

Definition 4.4 ([24]). A set of points $\mathcal{X} = \{t_1, \dots, t_n\} \subset \mathbb{R}^d$ is called m-unisolvent if the only polynomial of total degree at most m interpolating zero data on $\mathcal{X}$ is the zero polynomial.

We are ready to ensure the well-posed of interpolation problem under the conditions of following theorem [24]:

Theorem 4.5. *If the real-valued even function Φ is strictly conditionally positive definite of order m on $\mathbb{R}^d$ and the points $\{t_1, \dots, t_n\}$ form an $(m-1)$-unisolvent set, then the system of linear equations* (12) *is uniquely solvable.*

The following are some of the most widely used RBFs [24]:

- Gaussian (GA):

$$\phi(r) = e^{-c\|r\|^2}, \quad c > 0,$$

  which is strictly positive definite on $\mathbb{R}^d$.
- Inverse Multiquadrics (IMQ):

$$\phi(r) = \left(\|r\|^2 + c^2\right)^{-1/2}, \quad c > 0,$$

  also strictly positive definite on $\mathbb{R}^d$.
- Multiquadrics (MQ):

$$\phi(r) = \left(\|r\|^2 + c^2\right)^{1/2}, \quad c > 0,$$

  which is conditionally positive definite of order $m \geq 1$ in $\mathbb{R}^d$.
- Thin Plate Splines (TPS):

$$\phi(r) = (-1)^{n+1}\|r\|^{2n} \log \|r\|, \quad n \in \mathbb{N},$$

  which is conditionally positive definite of order $m \geq n+1$ in $\mathbb{R}^d$.

Next, we introduce a class of functions closely associated with conditionally positive definite radial functions, which provides a fundamental characterization of these functions.

Definition 4.6 ([24]). A function $\phi : [0, \infty) \to \mathbb{R}$ belonging to $C[0, \infty) \cap C^{\infty}(0, \infty)$ is considered completely monotone if it satisfies:

$$(-1)^l \phi^{(l)}(r) \geqslant 0, \quad r > 0, \quad l = 0, 1, 2, \dots$$

It's worth noting that the choice of the shape parameter influence significantly the success of the RBF method. In fact, this parameter is critical in controlling the behavior of the functions. However, determining an optimal value for the parameter c remains an ongoing research challenge. Several studies have explored this issue [21, 22, 25–27], yet a universally accepted solution is still challenging.

5 The computational scheme

We dedicate the current section to presenting a solving approach to approximate solutions of Eq. (1) using the RBF approach. RBFs are among the more advanced mesh-free methods that have received attention over the last few years and represent an essential tool for multivariate interpolation. Let us now use the RBF estimation scheme to solve problem (1). To accomplish this, we use an RBF and nodes in $[a, b]$. Thus, we define

$$\phi_j(t) = \Phi\Big(\Big|t - t_j\Big|\Big).$$

For ease of calculation, let us take $\theta(t) = \upsilon t$. By applying the fractional integral introduced in the preliminaries to both sides of Eq. (1), we may reformulate (1) in the following way

$$\begin{aligned} u(t) - \frac{1}{\Gamma(\alpha)} \int_0^t (t-s)^{\alpha-1} \Bigg[& a_1(s)u(s) + a_2(s)u(\upsilon s) \\ & + a_3(s) \int_0^s K_1(s, y)u(y)\mathrm{d}y \\ & + a_4(s) \int_0^{\upsilon s} K_2(s, \tau)u(\tau)\mathrm{d}\tau \Bigg] \mathrm{d}s = F(t), \end{aligned} \tag{14}$$

in which $F(t) = \lambda + \frac{1}{\Gamma(\alpha)} \int_0^t (t-s)^{\alpha-1} f(s)\mathrm{d}s$.

By utilizing the quadrature rule, we can evaluate the Eq. (14). First, instead of integrating in $[0, t]$, we integrate in the interval [0,1]. To accomplish this, we need to perform the conversion below

$$s := xt, \quad x \in [0, 1], \quad s \in [0, t]. \tag{15}$$

Next, we have

$$u(t) - \frac{t}{\Gamma(\alpha)} \int_0^1 (t - xt)^{\alpha-1} \Bigg[a_1(xt)u(xt) + a_2(xt)u(\upsilon xt) + a_3(xt) \int_0^{xt} K_1(xt, y)u(y)\mathrm{d}y + a_4(xt) \int_0^{\upsilon xt} K_2(xt, \tau)u(\tau)\mathrm{d}\tau \Bigg] \mathrm{d}x = F(t). \tag{16}$$

By analogy to the previous scheme, the integration distance $[0, \upsilon xt]$ and $[0, xt]$ are modified into the fixed distance in [0,1]. Therefore, we let

$$\begin{aligned} &y = xtq, \quad q \in [0,1], \quad y \in [0, xt], \\ &\tau = \upsilon xtr, \quad r \in [0,1], \quad \tau \in [0, \upsilon xt]. \end{aligned} \tag{17}$$

We obtain

$$u(t) - \frac{t}{\Gamma(\alpha)} \int_0^1 (t - xt)^{\alpha-1} \Bigg[a_1(xt)u(xt) + a_2(xt)u(\upsilon xt) + a_3(xt)xt \int_0^1 K_1(xt, xtq)u(xtq)\mathrm{d}q + a_4(xt)\upsilon xt \int_0^1 K_2(xt, \upsilon xtr)u(\upsilon xtr)\mathrm{d}r \Bigg] \mathrm{d}x = F(t). \tag{18}$$

For using the novel proposed technique, based on the RBF collocation scheme, for estimating the solution of problem (1), the Eq. (18) needs to be reduced to a system of equations. Subsequently, we use

$$\tilde{u}(t) = \sum_{j=1}^{n} d_j \phi_j(t) + \sum_{r=1}^{M} b_r p_r(t), \quad t \in [a, b], \tag{19}$$

to replace $u(t)$ as an approximation, i.e,

$$\tilde{u}(t) - \frac{t}{\Gamma(\alpha)} \int_0^1 (t - xt)^{\alpha-1} \Bigg[a_1(xt)\tilde{u}(xt) + a_2(xt)\tilde{u}(\upsilon xt) + a_3(xt)xt \int_0^1 K_1(xt, xtq)\tilde{u}(xtq)\mathrm{d}q + a_4(xt)\upsilon xt \int_0^1 K_2(xt, \upsilon xtr)\tilde{u}(\upsilon xtr)\mathrm{d}r \Bigg] \mathrm{d}x = F(t). \tag{20}$$

By substituting, we get

$$\begin{aligned} &\sum_{j=1}^{n} d_j \phi_j(t) + \sum_{r=1}^{M} b_r p_r(t) - \frac{t}{\Gamma(\alpha)} \int_0^1 (t - xt)^{\alpha-1} \\ &\times \Bigg[a_1(xt) \Bigg(\sum_{j=0}^{n} d_j \phi_j(xt) + \sum_{r=1}^{M} b_r p_r(xt) \Bigg) \\ &+ a_2(xt) \Bigg(\sum_{j=0}^{n} d_j \phi_j(\upsilon xt) + \sum_{r=1}^{M} b_r p_r(\upsilon xt) \Bigg) \\ &+ a_3(xt)xt \int_0^1 K_1(xt, xtq) \Bigg(\sum_{j=0}^{n} d_j \phi_j(xtq) + \sum_{r=1}^{M} b_r p_r(xtq) \Bigg) \mathrm{d}q \\ &+ a_4(xt)\upsilon xt \int_0^1 K_2(xt, \upsilon xtr) \Bigg(\sum_{j=0}^{n} d_j \phi_j(\upsilon xtr) + \sum_{r=1}^{M} b_r p_r(\upsilon xtr) \Bigg) \mathrm{d}r \Bigg] \mathrm{d}x = F(t). \end{aligned} \tag{21}$$

To evaluate the integral in (21), consider that the collocation points are the set of quadrature rule points $\{t_i\}_{i=1}^{n}$. Assume that Eq. (21) is valid at the collocation points, then

$$\begin{aligned} &\sum_{j=1}^{n} d_j \phi_j(t_i) + \sum_{r=1}^{M} b_r p_r(t_i) - \frac{t_i}{\Gamma(\alpha)} \int_0^1 (t_i - xt_i)^{\alpha-1} \\ &\times \Bigg[a_1(xt_i) \Bigg(\sum_{j=0}^{n} d_j \phi_j(xt_i) + \sum_{r=1}^{M} b_r p_r(xt_i) \Bigg) \\ &+ a_2(xt_i) \Bigg(\sum_{j=0}^{n} d_j \phi_j(\upsilon xt_i) + \sum_{r=1}^{M} b_r p_r(\upsilon xt_i) \Bigg) \\ &+ a_3(xt_i)xt_i \int_0^1 K_1(xt_i, xt_i q) \Bigg(\sum_{j=0}^{n} d_j \phi_j(xt_i q) + \sum_{r=1}^{M} b_r p_r(xt_i q) \Bigg) \mathrm{d}q \\ &+ a_4(xt_i)\upsilon xt_i \int_0^1 K_2(xt_i, \upsilon xt_i r) \Bigg(\sum_{j=0}^{n} d_j \phi_j(\upsilon xt_i r) \Bigg) \\ &+ \Bigg(\sum_{r=1}^{M} b_r p_r(\upsilon xt_i r) \Bigg) \mathrm{d}r \Bigg] \mathrm{d}x = F(t_i). \end{aligned} \tag{22}$$

The objective is to find an approximate vales of the integral terms of (22). For this, we use a uniform subdivision L to

generate m-point Gauss-Legendre quadrature. Note them $\{t_k\} = \{(t_{1_k}, \dots, t_{d_k})\}$ and the integration weights $\{w_k\}$. Based on results of [28], we get the following approximation

$$\int_{\Omega} K(x_i, t)\phi_j(t)\mathrm{d}t \approx \sum_{r=1}^{L}\sum_{k=1}^{m} \tilde{\mathbf{w}}_k K(x_i, \lambda_k^r)\phi_j(\lambda_k^r), \tag{23}$$

where $\tilde{\mathbf{w}}_k$ and $\lambda_k^r = \left(\lambda_{1_k}^r, \dots, \lambda_{d_k}^r\right)$ are calculated taking into account the weights $\{w_k\}$ and the points $\{t_k\}$. Consequently, the equation (22) may be formulated according to this numerical integration rule, and we get the next system of equations

$$\begin{aligned}
F(t_i) = {} & \sum_{j=1}^{n} \hat{d}_j\phi_j(t_i) + \sum_{r=1}^{M} \hat{b}_r p_r(t_i) \\
& - \frac{t_i}{\Gamma(\alpha)} \sum_{r_1=1}^{L}\sum_{k_1=1}^{m} \tilde{\mathbf{w}}_{k_1}\left(t_i - \lambda_{k_1}^{r_1} t_i\right)^{\alpha-1} \\
& \times \left(a_1\left(\lambda_{k_1}^{r_1} t_i\right)\left(\sum_{j=1}^{n} \hat{d}_j\phi_j\left(\lambda_{k_1}^{r_1} t_i\right) + \sum_{r=1}^{M} \hat{b}_r p_r\left(\lambda_{k_1}^{r_1} t_i\right)\right)\right. \\
& + a_2\left(\lambda_{k_1}^{r_1} t_i\right)\left(\sum_{j=1}^{n} \hat{d}_j\phi_j\left(\upsilon\lambda_{k_1}^{r_1} t_i\right) + \sum_{r=1}^{M} \hat{b}_r p_r\left(\upsilon\lambda_{k_1}^{r_1} t_i\right)\right) \\
& + a_3\left(\lambda_{k_1}^{r_1} t_i\right)\lambda_{k_1}^{r_1} t_i \sum_{r_2=1}^{L}\sum_{k_2=1}^{m} \tilde{\mathbf{w}}_{k_2} K_1\left(\lambda_{k_1}^{r_1} t_i, \lambda_{k_1}^{r_1} t_i \lambda_{k_2}^{r_2}\right) \\
& \times \left(\sum_{j=1}^{n} \hat{d}_j\phi_j\left(\lambda_{k_1}^{r_1} t_i\lambda_{k_2}^{r_2}\right) + \sum_{r=1}^{M} \hat{b}_r p_r\left(\lambda_{k_1}^{r_1} t_i\lambda_{k_2}^{r_2}\right)\right) \\
& + a_4\left(\lambda_{k_1}^{r_1} t_i\right)\upsilon\lambda_{k_1}^{r_1} t_i \sum_{r_3=1}^{L}\sum_{k_3=1}^{m} \tilde{\mathbf{w}}_{k_3} K_2\left(\lambda_{k_1}^{r_1} t_i, \upsilon\lambda_{k_1}^{r_1} t_i\lambda_{k_3}^{r_3}\right) \\
& \left.\times \left(\sum_{j=1}^{n} \hat{d}_j\phi_j\left(\upsilon\lambda_{k_1}^{r_1} t_i\lambda_{k_3}^{r_3}\right) + \sum_{r=1}^{M} \hat{b}_r p_r\left(\upsilon\lambda_{k_1}^{r_1} t_i\lambda_{k_3}^{r_3}\right)\right)\right).
\end{aligned} \tag{24}$$

To determine the unknown coefficients $\hat{d}_j$ and $\hat{b}_r$ from n equations resulting from (24), a set of M extra equations is needed, that is

$$\sum_{i=1}^{n} \hat{d}_i p_r(t_i) = 0, \quad 1 \le r \le M.$$

To determine the unknown coefficients $\hat{d}_j$ and $\hat{b}_r$, one can employ computational tools and suitable numerical algorithms to solve the given system efficiently. In conclusion, $u(t)$ may be estimated at every point $t \in [a, b]$ using

$$\hat{u}(t) = \sum_{j=1}^{n} \hat{d}_j\phi_j(t) + \sum_{r=1}^{M} \hat{b}_r p_r(t).$$

Now, we turn to a description of the method for the nonlinear case. By using the transformations (15) and (17), we can reformulate (2) as follows

$$\begin{aligned}
u(t) - \frac{t}{\Gamma(\alpha)} \int_0^1 (t - xt)^{\alpha-1} \big[& a_1(xt)u(xt) + a_2(xt)u(\upsilon xt) \\
& + a_3(xt)xt \int_0^1 K_1(xt, xtq)G_1(u(xtq))\mathrm{d}q \\
& + a_4(xt)\upsilon xt \int_0^1 K_2(xt, \upsilon xtr)G_2(u(\upsilon xtr))\mathrm{d}r \Big]\mathrm{d}x \\
& = G(t),
\end{aligned} \tag{25}$$

in which $G(t) = \lambda + \frac{1}{\Gamma(\alpha)}\int_0^t (t - s)^{\alpha-1} g(s)\mathrm{d}s$.

For using the novel proposed technique, based on the RBF collocation scheme, for estimating the solution of problem (2), the Eq. (25) needs to be reduced to an algebraic system of equations. Subsequently, we have

$$u^\star(t) = \sum_{j=1}^{n} d_j\phi_j(t) + \sum_{r=1}^{M} b_r p_r(t), \quad t \in [a, b], \tag{26}$$

as an estimate of $u(t)$, i.e,

$$\begin{aligned}
u^\star(t) - \frac{t}{\Gamma(\alpha)} \int_0^1 (t - xt)^{\alpha-1} \big[& a_1(xt)u^\star(xt) \\
& + a_2(xt)u^\star(\upsilon xt) + a_3(xt)xt \\
& \times \int_0^1 K_1(xt, xtq)G_1(u^\star(xtq))\mathrm{d}q \\
& + a_4(xt)\upsilon xt \int_0^1 K_2(xt, \upsilon xtr) \\
& \times G_2(u^\star(\upsilon xtr))\mathrm{d}r\big]\mathrm{d}x = G(t).
\end{aligned} \tag{27}$$

By substituting, we get

$$\begin{aligned}
& \sum_{j=1}^{n} d_j\phi_j(t) + \sum_{r=1}^{M} b_r p_r(t) \\
& \quad - \frac{t}{\Gamma(\alpha)} \int_0^1 (t - xt)^{\alpha-1}\left(a_1(xt)\left(\sum_{j=1}^{n} d_j\phi_j(xt)\right.\right. \\
& \quad \left. + \sum_{r=1}^{M} b_r p_r(xt)\right)
\end{aligned}$$

$$
\begin{aligned}
&+ a_2(xt)\left(\sum_{j=1}^{n} d_j\phi_j(\upsilon xt) + \sum_{r=1}^{M} b_r p_r(\upsilon xt)\right)\\
&+ a_3(xt)xt\int_0^1 K_1(xt, xtq)G_1\left(\sum_{j=1}^{n} d_j\phi_j(xtq)\right.\\
&\left.+ \sum_{r=1}^{M} b_r p_r(xtq)\right)\mathrm{d}q\\
&+ a_4(xt)\upsilon xt\int_0^1 K_2(xt, \upsilon xtr)G_2\left(\sum_{j=1}^{n} d_j\phi_j(\upsilon xtr)\right.\\
&\left.+ \sum_{r=1}^{M} b_r p_r(\upsilon xtr)\right)\mathrm{d}r\Bigg)\mathrm{d}x = G(t). \qquad (28)
\end{aligned}
$$

To evaluate the integral in (28), consider that the collocation points are the set of quadrature rule points $\{t_i\}_{i=1}^{n}$. Assume that Eq. (28) is valid at the collocation points, hence

$$
\begin{aligned}
&\sum_{j=1}^{n} d_j\phi_j(t_i) + \sum_{r=1}^{M} b_r p_r(t_i)\\
&\quad - \frac{t_i}{\Gamma(\alpha)}\int_0^1 (t_i - xt_i)^{\alpha-1}\left(a_1(xt_i)\left(\sum_{j=1}^{n} d_j\phi_j(xt_i)\right.\right.\\
&\quad\left.\left.+ \sum_{r=1}^{M} b_r p_r(xt_i)\right)\right.\\
&\quad\left. + a_2(xt_i)\left(\sum_{j=1}^{n} d_j\phi_j(\upsilon xt_i) + \sum_{r=1}^{M} b_r p_r(\upsilon xt_i)\right)\right.\\
&\quad\left. + a_3(xt_i)xt_i\int_0^1 K_1(xt_i, xt_iq)G_1\left(\sum_{j=1}^{n} d_j\phi_j(xt_iq)\right.\right.\\
&\quad\left.\left.+ \sum_{r=1}^{M} b_r p_r(xt_iq)\right)\mathrm{d}q\right.\\
&\quad\left. + a_4(xt_i)\upsilon xt_i\int_0^1 K_2(xt_i, \upsilon xt_ir)G_2\left(\sum_{j=1}^{n} d_j\phi_j(\upsilon xt_ir)\right.\right.\\
&\quad\left.\left.+ \sum_{r=1}^{M} b_r p_r(\upsilon xt_ir)\right)\mathrm{d}r\right)\mathrm{d}x = G(t_i). \qquad (29)
\end{aligned}
$$

The integral terms in (29) can be numerically approximated using the Gauss-Legendre quadrature rule with m points. To achieve this, we divide the domain into L uniform subintervals, where each subdivision contains integration nodes given by $\{t_k\} = \{(t_{1_k}, \ldots, t_{d_k})\}$, along with their associated weights $\{w_k\}$. By using (23), the equation (29) may be formulated into a system of algebraic equations

$$
\begin{aligned}
G(t_i) &= \sum_{j=1}^{n} \hat{d}_j\phi_j(t_i) + \sum_{r=1}^{M} \hat{b}_r p_r(t_i)\\
&\quad - \frac{t_i}{\Gamma(\alpha)}\sum_{r_1=1}^{L}\sum_{k_1=1}^{m} \tilde{\mathbf{w}}_{k_1}\left(t_i - \lambda_{k_1}^{r_1}t_i\right)^{\alpha-1}\\
&\quad\times\left(a_1\left(\lambda_{k_1}^{r_1}t_i\right)\left(\sum_{j=1}^{n} \hat{d}_j\phi_j\left(\lambda_{k_1}^{r_1}t_i\right)\right.\right.\\
&\quad\left.\left.+ \sum_{r=1}^{M} \hat{b}_r p_r\left(\lambda_{k_1}^{r_1}t_i\right)\right)\right.\\
&\quad\left. + a_2\left(\lambda_{k_1}^{r_1}t_i\right)\left(\sum_{j=1}^{n} \hat{d}_j\phi_j\left(\upsilon\lambda_{k_1}^{r_1}t_i\right)\right.\right.\\
&\quad\left.\left.+ \sum_{r=1}^{M} \hat{b}_r p_r\left(\upsilon\lambda_{k_1}^{r_1}t_i\right)\right)\right.\\
&\quad\left. + a_3\left(\lambda_{k_1}^{r_1}t_i\right)\lambda_{k_1}^{r_1}t_i\sum_{r_2=1}^{L}\sum_{k_2=1}^{m} \tilde{\mathbf{w}}_{k_2}\right.\\
&\quad\times K_1\left(\lambda_{k_1}^{r_1}t_i, \lambda_{k_1}^{r_1}t_i\lambda_{k_2}^{r_2}\right)G_1\left(\sum_{j=1}^{n} \hat{d}_j\phi_j\left(\lambda_{k_1}^{r_1}t_i\lambda_{k_2}^{r_2}\right)\right.\\
&\quad\left.\left.+ \sum_{r=1}^{M} \hat{b}_r p_r\left(\lambda_{k_1}^{r_1}t_i\lambda_{k_2}^{r_2}\right)\right)\right.\\
&\quad\left. + a_4\left(\lambda_{k_1}^{r_1}t_i\right)\upsilon\lambda_{k_1}^{r_1}t_i\sum_{r_3=1}^{L}\sum_{k_3=1}^{m} \tilde{\mathbf{w}}_{k_3}\right.\\
&\quad\times K_2\left(\lambda_{k_1}^{r_1}t_i, \upsilon\lambda_{k_1}^{r_1}t_i\lambda_{k_3}^{r_3}\right)G_2\left(\sum_{j=1}^{n} \hat{d}_j\phi_j\left(\upsilon\lambda_{k_1}^{r_1}t_i\lambda_{k_3}^{r_3}\right)\right.\\
&\quad\left.\left.\left.+ \sum_{r=1}^{M} \hat{b}_r p_r\left(\upsilon\lambda_{k_1}^{r_1}t_i\lambda_{k_3}^{r_3}\right)\right)\right)\right). \qquad (30)
\end{aligned}
$$

To determine the unknown coefficients $\hat{d}_j$ and $\hat{b}_r$ from n equations resulting from (30), a set of M extra equations is needed, that is

$$
\sum_{i=1}^{n} \hat{d}_i p_r(t_i) = 0, \quad 1 \le r \le M.
$$

Using a suitable solver, the coefficients $\hat{d}_j$ and $\hat{b}_r$ may be derived from (30). In conclusion, $u(t)$ may be estimated at every point $t \in [a, b]$ using

$$
\hat{u}^{\star}(t) = \sum_{j=1}^{n} \hat{d}_j\phi_j(t) + \sum_{r=1}^{M} \hat{b}_r p_r(t).
$$

6 Error analysis

Firstly, we present some fundamental results concerning the solvability and the qualitative proprieties of the solutions. In the case of $\alpha = n$ in Eq. (6), the regularity result of (1) holds by the lemma below.

Lemma 2 ([29]). *Suppose* $a_j(t)$ $(j = 1, 2, \dots, 4)$, $f(t) \in C^m(I), K_1 \in C^m(D)$ *and* $K_2 \in C^m(\tilde{D})$ *at any* $m \geq 0$. *Therefore,* (1) *has a unique solution* $u(t) \in C^{m+1}(I)$.

We define $C(I)$ as the Banach space and introduce several key concepts and assumptions that will be used throughout this section.

(M_1) Suppose that for each function $a_i(t) \in C(I)$ and for every $t \in I$, $\exists L_i$ where

$$|a_i(t)| \leq L_i, \quad \forall i = 1, 2, 3, 4,$$

where the maximum among these values is denoted as

$$\max\{L_i\} = L_a.$$

(M_2) Additionally, if there exist constants $\mathcal{M}_1$ and $\mathcal{M}_2$ satisfying

$$\mathcal{M}_1 = \max_{t\in I} \int_0^t |K_1(t,s)|\mathrm{d}s, \quad \mathcal{M}_2 = \max_{t\in I} \int_0^{\upsilon t} |K_2(t,\tau)|\mathrm{d}\tau,$$

then we define

$$\max\{\mathcal{M}_1, \mathcal{M}_2\} = \mathcal{M}.$$

Theorem 6.1 ([12]). *Given the conditions* (M_1) *and* (M_2), *if*

$$\frac{2b^\alpha L_a(1+\mathcal{M})}{\Gamma(\alpha+1)} < 1,$$

then $\exists u \in C(I)$ *a unique solution for* (14).

We now proceed to analyze the error estimation of the proposed method for solving (14). To begin, we introduce the fill distance parameter $h_{\mathcal{X},\Omega}$.

Definition 6.2 ([23]). Let Ω a bounded set, and $\mathcal{X} = \{t_i\}_{i=1}^n \subseteq \Omega$ a set of points then

$$h_{\mathcal{X},\Omega} = \sup_{t\in\Omega} \min_{t_j\in\mathcal{X}} \left\| t - t_j \right\|_2,$$

is the fill distance of $\mathcal{X}$

Definition 6.3 ([24]). Consider $\Phi \in C(\mathbb{R}^d) \cap L^1(\mathbb{R}^d)$ as a strictly positive definite function. The corresponding native Hilbert space is defined as

$$\aleph_\Phi(\mathbb{R}^d) = \left\{ u \in C(\mathbb{R}^d) \cap L^2(\mathbb{R}^d) : \frac{\hat{u}}{\sqrt{\hat{\Phi}}} \in L^2(\mathbb{R}^d) \right\},$$

equipped with the inner product

$$< u, v >_\Phi(\mathbb{R}^d) = \frac{1}{\sqrt{2\pi}} < \frac{\hat{u}}{\sqrt{\hat{\Phi}}}, \frac{\hat{v}}{\sqrt{\hat{\Phi}}} >_{L^2(\mathbb{R}^d)} = \frac{1}{\sqrt{2\pi}} \int_{\mathbb{R}^d} \frac{\hat{u}(\eta)\overline{\hat{v}(\eta)}}{\sqrt{\hat{\Phi}}} \mathrm{d}\eta,$$

where $\hat{u}$ represents the Fourier transform of u.

Theorem 6.4 ([24]). *If* $\Omega \subseteq (\mathbb{R})^d$ *is a bounded domain with an interior cone condition. Suppose that* Φ *is an infinitely smooth positive definite radial basis function (RBF). Then,* $\exists h_0(l) > 0$ *and* $C_l > 0$ *where*

$$\left\| u(t) - \mathcal{P}_n u(t) \right\|_{L^\infty(\Omega)} \leqslant C_l h_{\mathcal{X},\Omega}^l |u|_{\aleph_\Phi(\Omega)},$$

here $u \in \aleph_\Phi(\Omega)$, $\mathcal{P}_n u$ *is the interpolant of* u *over* $\mathcal{X}$, *and* $h_{\mathcal{X},\Omega} \leq h_0(l)$.

Remark 6.5 ([24]). Based on Theorem (6.4), for sufficiently small $h_{\mathcal{X},\Omega}$ and a positive constant c, the error bound for Gaussian approximation (GA) is given by

$$\Phi(t) = e^{(-c\|t\|^2)}, \quad c > 0,$$

which yields

$$\left\| u - \mathcal{P}_n u \right\|_{L^\infty(\Omega)} \leq e^{\left(-\frac{c\left|\log h_{\mathcal{X},\Omega}\right|}{h_{\mathcal{X},\Omega}}\right)} \|u\|_{\aleph_\Phi(\Omega)}. \tag{31}$$

In the case of inverse multiquadrics, where

$$\Phi(t) = \left(\|t\|^2 + c^2\right)^\beta, \quad c > 0, \quad \beta < 0,$$
$$or \quad \beta > 0 \quad and \quad \beta \notin \mathbb{N},$$

we obtain the following bound:

$$\left\| u - \mathcal{P}_n u \right\|_{L_\infty(\Omega)} \leq e^{\left(-\frac{c}{h_{\mathcal{X},\Omega}}\right)} \|u\|_{\aleph_\Phi(\Omega)}. \tag{32}$$

The problem (14) may be formulated in as a general operator form:

$$(I - \mathcal{K})u = F, \tag{33}$$

with the linear operator $\mathcal{K} : C(\Omega) \to C(\Omega)$ is expressed by

$$\mathcal{K}u(t) = \frac{1}{\Gamma(\alpha)} \int_0^t (t-s)^{\alpha-1} \Bigg[a_1(s)u(s) + a_2(s)u(\upsilon s) + a_3(s) \int_0^s K_1(s,y)u(y)\mathrm{d}y + a_4(s) \int_0^{\upsilon s} K_2(s,\tau)u(\tau)\mathrm{d}\tau \Bigg] \mathrm{d}s, \tag{34}$$

where I represents the identity operator.

Let $\mathcal{K}$ be a bounded operator mapping $C(\Omega)$ into itself, satisfying $\|\mathcal{K}\| < 1$. Under this condition, the operator $I - \mathcal{K}$ becomes a contraction. By applying the Banach fixed-point theorem, it follows that the equation (33) admits a unique solution $u^\star(t) \in C(\Omega)$ for any given function $F(t) \in C(\Omega)$. Moreover, invoking the geometric series theorem ([28]), we establish that the operator $I - \mathcal{K} : C(\Omega) \overset{1-1}{\underset{\text{onto}}{\to}} C(\Omega)$ possesses a bounded inverse, yielding the estimate

$$\left\| (I - \mathcal{K})^{-1} \right\| \leq \frac{1}{1 - \|\mathcal{K}\|}.$$

To discretize the problem, we define a projection operator $\mathcal{P}_n : C(\Omega) \to C_n(\Omega)$ associated with the collocation points $\{t_1, \ldots, t_n\} \subset \Omega$:

$$\mathcal{P}_n u(t) = \sum_{k=1}^{n} d_k \phi\big(\|t - t_k\|\big), \quad t \in \Omega.$$

Here, the function space $C_n(\Omega)$ is spanned by $\{\Phi_1, \ldots, \Phi_n\}$, and the coefficients $\{d_k\}$ are determined by solving the interpolation problem:

$$\mathcal{P}_n u(t_i) = u(t_i), \quad i = 1, \ldots, n.$$

Next, the corresponding system for the collocation method takes the following scheme:

$$(I - \mathcal{P}_n \mathcal{K}) u_n = \mathcal{P}_n F. \tag{35}$$

Incorporating numerical quadrature, we sequentially use integrals $\mathcal{K}_m$ defined as

$$\begin{aligned} \mathcal{K}_m u(t) = \frac{t}{\Gamma(\alpha)} \sum_{r_1=1}^{L} \sum_{k_1=1}^{m} \tilde{\mathbf{w}}_{k_1} \Big(t - \lambda_{k_1}^{r_1} t\Big)^{\alpha-1} \\ \times \Big(a_1\Big(\lambda_{k_1}^{r_1} t\Big) u\Big(\lambda_{k_1}^{r_1} t\Big) \\ + a_2\Big(\lambda_{k_1}^{r_1} t\Big) u\Big(\upsilon \lambda_{k_1}^{r_1} t\Big) + a_3\Big(\lambda_{k_1}^{r_1} t\Big) \lambda_{k_1}^{r_1} t \\ \times \sum_{r_2=1}^{L} \sum_{k_2=1}^{m} \tilde{\mathbf{w}}_{k_2} K_1\Big(\lambda_{k_1}^{r_1} t, \lambda_{k_1}^{r_1} t \lambda_{k_2}^{r_2}\Big) u\Big(\lambda_{k_1}^{r_1} t \lambda_{k_2}^{r_2}\Big) \\ + a_4\Big(\lambda_{k_1}^{r_1} t\Big) \upsilon \lambda_{k_1}^{r_1} t \sum_{r_3=1}^{L} \sum_{k_3=1}^{m} \tilde{\mathbf{w}}_{k_3} \\ \times K_2\Big(\lambda_{k_1}^{r_1} t, \upsilon \lambda_{k_1}^{r_1} t \lambda_{k_3}^{r_3}\Big) u\Big(\upsilon \lambda_{k_1}^{r_1} t \lambda_{k_3}^{r_3}\Big) \Big). \end{aligned} \tag{36}$$

Following [28, 30], we consider that $\mathcal{K}_m$ satisfies the next conditions:

- H_1: The sequence of operators $\mathcal{K}_m$ is a collectively compact family on $C(\Omega)$.
- H_2: The operator sequence $\mathcal{K}_m$ converges pointwise to $\mathcal{K}$ on $C(\Omega)$.

Additionally, for any function $u \in C^{(2n)}(\Omega)$ having non-singular kernel K, we get the bound [31]:

$$\|\mathcal{K} - \mathcal{K}_m\| \leq \frac{C_m}{L^{2m}} \sup_{t \in \Omega} \left| u^{(2m)}(t) \right|, \tag{37}$$

where $C_m > 0$ is a constant.

By utilizing (36) and incorporating (11), we express (24) as

$$(I - \mathcal{P}_n \mathcal{K}_m) \hat{u}_n = \mathcal{P}_n F. \tag{38}$$

To further refine the accuracy of the numerical solution, an iterated discrete collocation approach is introduced:

$$\bar{u}_n = F + \mathcal{P}_n \mathcal{K}_m \hat{u}_n. \tag{39}$$

From this formulation, it is straightforward to verify that

$$\mathcal{P}_n \bar{u}_n = \hat{u}_n.$$

Thus, we can conclude that

$$(I - \mathcal{K}_m \mathcal{P}_n) \bar{u}_n = F.$$

Theorem 6.6 ([28]). *Suppose that the operator sequence $\mathcal{K}_m$ in* (36) *satisfies assumptions H_1 and H_2. Let a class of projection operators noted by $\{\mathcal{P}_n\}$ that map $C(\Omega)$ into itself and assume that for every function $u \in C(\Omega)$, we have*

$$\mathcal{P}_n u \to u \quad \text{as } n \to \infty.$$

Let $u^\star$ be the unique solution of (14). *Then, the operator $\mathcal{K}_m \mathcal{P}_n$ is collectively compact and pointwise convergent on $C(\Omega)$. Moreover, for $n > N$, the inverse operator $\left(I - \mathcal{K}_m \mathcal{P}_n\right)^{-1}$ exists and remains uniformly bounded. Additionally, the approximate solution $\bar{u}_n$ verifies:*

$$\begin{aligned} \left\| \bar{u}_n - u^\star \right\|_{L^\infty(\Omega)} \leqslant \left\| \left(I - \mathcal{K}_m \mathcal{P}_n\right)^{-1} \right\| \\ \times \left\| \mathcal{K} u^\star - \mathcal{K}_n \mathcal{P}_n u^\star \right\|_{L^\infty(\Omega)}, \quad n \geqslant N. \end{aligned}$$

To establish convergence, we use the following result.

Theorem 6.7. *Assume that* $\exists! u^\star \in C^{(2m)}(\Omega) \cap \aleph_\Phi(\Omega)$ *solution of* (14)*. Suppose further that the proposed scheme is applied on a quasi-uniform set* $\mathcal{X} = \{t_i\}_{i=1}^n \subset \Omega$*, and that the conditions of Theorem* (6.4) *hold. Then,* $\exists N > 0$ *where* $\forall n > N$*, the method yields a unique solution* $\hat{u}_n$ *that converges to* $u^\star$ *as* $n \to \infty$*. Furthermore, there exist constants* ϱ_1 *and* ϱ_2 *such that*

$$\|\hat{u}_n - u^\star\|_{L^\infty(\Omega)} \leq \varrho_1 C_l h_{\mathcal{X},\Omega}^l \|u^\star\|_{\aleph_\phi(\Omega)} + \varrho_2 \frac{C_m}{L^{2m}} \sup_{t\in\Omega} \left| u^{\star(2m)}(t) \right|.$$

Proof. From Theorem (6.6), we know that the iterated approach possesses a solution $\bar{u}_n$, and that $\left(I - \mathcal{K}_m \mathcal{P}_n\right)^{-1}$ exists and is uniformly bounded. Hence, we assume

$$\left\| \left(I - \mathcal{K}_m \mathcal{P}_n\right)^{-1} \right\| \leqslant \rho_1 < \infty.$$

This leads to the estimate:

$$\begin{aligned} \|\bar{u}_n - u^\star\|_{L^\infty(\Omega)} &\leq \left\| \left(I - \mathcal{K}_m \mathcal{P}_n\right)^{-1} \right\| \\ &\quad \times \|\mathcal{K}u^\star - \mathcal{K}_m \mathcal{P}_n u^\star\|_{L^\infty(\Omega)} \\ &\leq \rho_1 \|\mathcal{K}u^\star - \mathcal{K}_m \mathcal{P}_n u^\star\|_{L^\infty(\Omega)} \\ &\leq \rho_1 \{ \|\mathcal{K}u^\star - \mathcal{K}_m u^\star\|_{L^\infty(\Omega)} \\ &\quad + \left\| \mathcal{K}_m \left(u^\star - \mathcal{P}_n u^\star\right) \right\|_{L^\infty(\Omega)} \}. \end{aligned}$$

By assumption H_2, for a large n, $\exists \rho_2 > 0$ verifying

$$\|\mathcal{K}_m\| \leqslant \rho_2 < \infty.$$

Consequently, we obtain:

$$\begin{aligned} \|\bar{u}_n - u^\star\|_{L^\infty(\Omega)} &\leq \rho_1 \{ \|\mathcal{K}u^\star - \mathcal{K}_m u^\star\|_{L^\infty(\Omega)} \\ &\quad + \rho_2 \|u^\star - \mathcal{P}_n u^\star\|_{L^\infty(\Omega)} \}. \end{aligned}$$

Using the definition of quasi-uniformity, we note that

$$h_{\mathcal{X},\Omega} \to 0, \quad \text{as} \quad n \to \infty.$$

Applying Theorem (6.4), we conclude that $\forall u^\star \in \aleph_\Phi(\Omega)$, $\exists h_0$ and C_l satisfying

$$\|u^\star - \mathcal{P}_n u^\star\|_{L^\infty(\Omega)} \leqslant C_l h_{\mathcal{X},\Omega}^l |u^\star|_{\aleph_\Phi(\Omega)}, \tag{40}$$

for all $t \in \Omega$, provided $h_{\mathcal{X},\Omega} \leq h_0(l)$.

Using the error bound from (37), we also obtain

$$\|\mathcal{K}u^\star - \mathcal{K}_m u^\star\|_{L^\infty(\Omega)} \leq \frac{C_m}{L^{2m}} \sup_{t\in\Omega} \left| u^{\star(2m)}(t) \right|. \tag{41}$$

This implies that $\mathcal{K}_m u^\star \to \mathcal{K}u^\star$ as $m \to \infty$.

By Theorem (31), we deduce:

$$\|\bar{u}_n - u^\star\|_{L^\infty(\Omega)} \leq \rho_1 \big(\|\mathcal{K}u^\star - \mathcal{K}_m u^\star\|_{L^\infty(\Omega)} + \rho_2 C_l h_{\mathcal{X},\Omega}^l \|u^\star\|_{\aleph_\phi(\Omega)} \big).$$

Finally, using (40) and (41), we conclude:

$$\|\hat{u}_n - u^\star\|_{L^\infty(\Omega)} \to 0, \quad \text{as} \quad n \to \infty.$$

□

Now, we turn to the analysis of the error estimation of the proposed method for the non-linear case.

Let us consider the abstract form of the Eq. (2) in the following way:

$$u = \mathcal{V}u + G,$$

with the integral operator $\mathcal{V} : C(\Omega) \to C(\Omega)$ is expressed by

$$\begin{aligned} \mathcal{V}u(t) = \frac{t}{\Gamma(\alpha)} \int_0^1 (t - xt)^{\alpha-1} \Bigg[& a_1(xt)u(xt) + a_2(xt)u(\upsilon xt) \\ & + a_3(xt)xt \int_0^1 K_1(xt, xtq) G_1(u(xtq)) \mathrm{d}q \\ & + a_4(xt)\upsilon xt \int_0^1 K_2(xt, \upsilon xtr) G_2(u(\upsilon xtr)) \mathrm{d}r \Bigg] \mathrm{d}x. \end{aligned} \tag{42}$$

Subsequently, the system related to the collocation method corresponds to the abstract form

$$\left(I - \mathcal{P}_n \mathcal{V}\right) u_n = \mathcal{P}_n G. \tag{43}$$

By applying the quadrature formula to the coefficients $\left\{ \lambda_{k_i}^{r_i} \right\}$, $i = 1, \ldots, 3$ and weights $\left\{ \tilde{\mathbf{w}}_{k_i} \right\}$, $i = 1, \ldots, 3$, we introduce the operators $\mathcal{V}_n$ defined by

$$\begin{aligned} \mathcal{V}_n u(t) = \frac{t}{\Gamma(\alpha)} \sum_{r_1=1}^{L} \sum_{k_1=1}^{m} \tilde{\mathbf{w}}_{k_1} \left(t - \lambda_{k_1}^{r_1} t \right)^{\alpha-1} & \\ \times \Big(a_1\Big(\lambda_{k_1}^{r_1} t\Big) u\Big(\lambda_{k_1}^{r_1} t\Big) & \\ + a_2\Big(\lambda_{k_1}^{r_1} t\Big) u\Big(\upsilon \lambda_{k_1}^{r_1} t\Big) & \\ + a_3\Big(\lambda_{k_1}^{r_1} t\Big) \lambda_{k_1}^{r_1} t \sum_{r_2=1}^{L} \sum_{k_2=1}^{m} \tilde{\mathbf{w}}_{k_2} & \\ \times K_1\Big(\lambda_{k_1}^{r_1} t, \lambda_{k_1}^{r_1} t \lambda_{k_2}^{r_2}\Big) G_1\Big(u\Big(\lambda_{k_1}^{r_1} t \lambda_{k_2}^{r_2}\Big)\Big) & \\ + a_4\Big(\lambda_{k_1}^{r_1} t\Big) \upsilon \lambda_{k_1}^{r_1} t \sum_{r_3=1}^{L} \sum_{k_3=1}^{m} \tilde{\mathbf{w}}_{k_3} & \\ \times K_2\Big(\lambda_{k_1}^{r_1} t, \upsilon \lambda_{k_1}^{r_1} t \lambda_{k_3}^{r_3}\Big) G_2\Big(u\Big(\upsilon \lambda_{k_1}^{r_1} t \lambda_{k_3}^{r_3}\Big)\Big)\Big). & \end{aligned} \tag{44}$$

By using (11) and (44), we can rewrite (30) in the form of an operator as follows

$$\left(I - \mathcal{P}_n\mathcal{V}_n\right)\hat{u}_n = \mathcal{P}_n G. \tag{45}$$

Consider $\mathcal{Q}_n$, the operator described as follows

$$\mathcal{Q}_n u = \mathcal{P}_n\mathcal{V}u + \mathcal{P}_n G.$$

Then, (43) can be written as

$$u_n = \mathcal{Q}_n u_n.$$

Let's also assume that $\hat{\mathcal{Q}}_n$ is the operator given by

$$\hat{\mathcal{Q}}_n u = \mathcal{P}_n\mathcal{V}_n u + \mathcal{P}_n G.$$

Then (45) can be written as

$$\hat{u}_n = \hat{\mathcal{Q}}_n\hat{u}_n.$$

The error analysis of the presented scheme can be obtained by applying the theorem from Vainikko [32].

Theorem 6.8 ([32]). *Consider an open set Ω within a Banach space $\mathcal{X}$, where the continuous operators Q and $\tilde{Q}$ are defined. Suppose the equation*

$$u = \tilde{Q}u$$

admits an isolated solution $\tilde{u}_0$ in Ω, and the following conditions hold:

(a) The operator Q is Fréchet differentiable in a neighborhood of $\tilde{u}_0$, and the linear operator $I - Q'(\tilde{u}_0)$ is continuously invertible.

(b) There exist constants $\eta > 0$ and $0 < \rho < 1$ such that certain inequalities hold, where η is chosen sufficiently small to ensure that the sphere $\|u - \tilde{u}_0\| \le \eta$ remains within Ω.

$$\sup_{\|u-\tilde{u}_0\|\le\eta} \left\| \left(I - Q'(\tilde{u}_0)\right)^{-1}\left(Q'(u) - Q'(\tilde{u}_0)\right)\right\| \le \rho, \tag{46}$$

$$x = \left\| \left(I - Q'(\tilde{u}_0)\right)^{-1}\left(Q(\tilde{u}_0) - \tilde{Q}(\tilde{u}_0)\right)\right\| \le \eta(1-\rho), \tag{47}$$

therefore the equation $u = Qu$ has a unique solution u_0 in the sphere $\|u - \tilde{u}_0\| \le \eta$. Furthermore, the inequality

$$\frac{x}{1+\rho} \le \|u_0 - \tilde{u}_0\| \le \frac{x}{1-\rho},$$

is valid.

Theorem 6.9. *Consider an isolated solution $u_0 \in C[0,1]$ of the equation*

$$u = \mathcal{V}u + G.$$

Suppose that the linear operator $\mathcal{Q}'(u_0)$ does not have 1 as an eigenvalue. Then, for a large n, the inverse of the operator $\left(I - \hat{\mathcal{Q}}_n'(u_0)\right)$ exists, and there exists a constant $N > 0$, independent of n, such that

$$\left\| \left(I - \hat{\mathcal{Q}}_n'(u_0)\right)^{-1}\right\| \le N.$$

The subsequent theorem establishes the necessary conditions for the existence of an approximate solution $\hat{u}_n$ near u_0.

Theorem 6.10. *Let $u_0 \in C([0,1]\times[0,1])$ be an isolated solution of*

$$u = \mathcal{V}u + G.$$

Assume that $\mathcal{P}_n$ represents an interpolatory projection and that the linear operator $\mathcal{Q}'(u_0)$ does not have 1 as an eigenvalue. Then, for a large n, a unique approximate solution $\hat{u}_n$ to (45) exists in the ball

$$B(u_0,\eta) = \left\{u\colon \|u - u_0\| \le \eta\right\},$$

for some $\eta > 0$. Moreover, $\exists 0 < \rho < 1$ that remains independent of n, ensuring that

$$\frac{y_n}{1+\rho} \le \|u_0 - \hat{u}_n\| \le \frac{y_n}{1-\rho},$$

where

$$y_n = \left\| \left(I - \hat{\mathcal{Q}}_n'(u_0)\right)^{-1}\left(\hat{\mathcal{Q}}_n(u_0) - \mathcal{Q}(u_0)\right)\right\|.$$

Proof. Theorem (6.9) assures us that $\left(I - \hat{\mathcal{Q}}'_n(u_0)\right)^{-1}$ exists and is uniformly bounded, which means that there is a constant $N > 0$ so that

$$\left\| \left(I - \hat{\mathcal{Q}}_n'(u_0)\right)^{-1}\right\| \le N.$$

Furthermore, according to the uniform boundedness principle for RBF, it follows that $\|\mathcal{P}_n\| \le \kappa$, and Moreover, we have $\|\mathcal{V}_n'\| \le \gamma$ for all $u \in B(u_0,\eta)$ hence

$$\begin{aligned}\left\|\hat{\mathcal{Q}}_n'(u) - \hat{\mathcal{Q}}_n'(u_0)\right\| &= \|\mathcal{P}_n\mathcal{V}_n'u - \mathcal{P}_n\mathcal{V}_n'u_0\| \\ &\le \|\mathcal{P}_n\|\|\mathcal{V}_n'u - \mathcal{V}_n'u_0\| \le \kappa\gamma\eta.\end{aligned}$$

Thus, we have

$$\begin{aligned}&\sup_{\|u-\tilde{u}_0\|\le\eta,} \left\| \left(I - \hat{\mathcal{Q}}'_n(u_0)\right)^{-1}\left(\hat{\mathcal{Q}}'_n(u) - \hat{\mathcal{Q}}'_n(u_0)\right)\right\| \\ &\quad \le \mathrm{N}\kappa\gamma\eta \le \rho,\end{aligned}$$

with $0 < \rho < 1$, demonstrates the relation (46) of theorem (6.8) for η small enough. In addition, it yields

$$
\begin{aligned}
y_n &= \left\| \left(I - \hat{\mathcal{Q}}'_n(u_0)\right)^{-1} \left(\hat{\mathcal{Q}}_n(u_0) - \mathcal{Q}(u_0)\right) \right\| \\
&\leq \left\| \left(I - \hat{\mathcal{Q}}'_n(u_0)\right)^{-1} \right\| \left\| \hat{\mathcal{Q}}_n(u_0) - \mathcal{Q}(u_0) \right\| \\
&\leq N \left\| \hat{\mathcal{Q}}_n(u_0) - \mathcal{Q}(u_0) \right\|.
\end{aligned}
$$

Now, we want to prove that $\left\| \hat{\mathcal{Q}}_n(u_0) - \mathcal{Q}(u_0) \right\| \to 0$ as $n \to \infty$. We have

$$
\begin{aligned}
\left\| \hat{\mathcal{Q}}_n(u_0) - \mathcal{Q}(u_0) \right\| &= \| \mathcal{P}_n \mathcal{V}_n u_0 + \mathcal{P}_n G - \mathcal{V} u_0 - G \| \\
&= \| \mathcal{P}_n \mathcal{V}_n u_0 + \mathcal{P}_n G - \mathcal{V} u_0 - G \\
&\quad + \mathcal{P}_n(\mathcal{V} u_0 + G) - \mathcal{P}_n(\mathcal{V} u_0 + G) \| \\
&\leq \| \mathcal{P}_n \{ \mathcal{V}_n u_0 + G - \mathcal{V} u_0 - G \} \| \\
&\quad + \left\| (\mathcal{P}_n - I)(\mathcal{V} u_0 + G) \right\| \\
&\leq \kappa \| \mathcal{V}_n - \mathcal{V} \| \| u_0 \| + \| \mathcal{P}_n u_0 - u_0 \| \\
&\quad \to 0 \text{ when } n \to \infty.
\end{aligned} \tag{48}
$$

Let n be large enough, we have $y_n \leq \eta(1 - \rho)$. Consequently, relation (47) of theorem (6.8) is fulfilled. Using theorem (6.8), it follows that

$$
\frac{y_n}{1+\rho} \leq \| \hat{u}_n - u_0 \| \leq \frac{y_n}{1-\rho}.
$$

The proof is complete. □

Theorem 6.11. *Consider $u_0 \in \aleph_\Phi(\Omega)$ as an isolated solution of (25) and $\hat{u}_n$ be the RBFs collocation estimate of u_0.*

Hence, for the inverse multiquadrics (IMQ), we have

$$
\begin{aligned}
\| \hat{u}_n - u_0 \|_{L^\infty(\Omega)} &\leq \frac{N\kappa}{1-\rho} \| \mathcal{V}_n u_0 - \mathcal{V} u_0 \|_{L^\infty(\Omega)} \\
&\quad + \frac{N}{1-\rho} e^{\left(-\frac{c}{h_{\mathcal{X},\Omega}}\right)} \| u_0 \|_{\aleph_\Phi(\Omega)}.
\end{aligned}
$$

In the same way, we get for the Gaussians (GA)

$$
\begin{aligned}
\| \hat{u}_n - u_0 \|_{L^\infty(\Omega)} &\leq \frac{N\kappa}{1-\rho} \| \mathcal{V}_n u_0 - \mathcal{V} u_0 \|_{L^\infty(\Omega)} \\
&\quad + \frac{N}{1-\rho} e^{\frac{-c|\log h_{\mathcal{X},\Omega}|}{h_{\mathcal{X},\Omega}}} \| u_0 \|_{\aleph_\Phi(\Omega)}.
\end{aligned}
$$

Proof. According to theorem (6.10), we obtain

$$
\| \hat{u}_n - u_0 \| \leq \frac{y_n}{1-\rho}.
$$

Using remark (6.5), theorem (6.9) and estimation (48), we obtain the following results

$$
\begin{aligned}
&\| \hat{u}_n - u_0 \|_{L^\infty(\Omega)} \\
&\quad \leq \frac{y_n}{1-\rho} = \frac{\left\| \left(I - \hat{\mathcal{Q}}'_n(u_0)\right)^{-1} \left(\hat{\mathcal{Q}}_n(u_0) - \mathcal{Q}(u_0)\right) \right\|_{L^\infty(\Omega)}}{1-\rho} \\
&\quad \leq \frac{N}{1-\rho} \left\| \hat{\mathcal{Q}}_n(u_0) - \mathcal{Q}(u_0) \right\|_{L^\infty(\Omega)} \\
&\quad \leq \frac{N}{1-\rho} \| \mathcal{P}_n \|_{L^\infty(\Omega)} \| \mathcal{V}_n - \mathcal{V} \|_{L^\infty(\Omega)} \\
&\qquad \times \| u_0 \|_{L^\infty(\Omega)} + \frac{N}{1-\rho} \| \mathcal{P}_n u_0 - u_0 \|_{L^\infty(\Omega)} \\
&\quad \leq \frac{N\kappa}{1-\rho} \| \mathcal{V}_n - \mathcal{V} \|_{L^\infty(\Omega)} \| u_0 \|_{L^\infty(\Omega)} \\
&\qquad + \frac{N}{1-\rho} e^{\frac{-c|\log h_{\mathcal{X},\Omega}|}{h_{\mathcal{X},\Omega}}} \| u_0 \|_{\aleph_\Phi(\Omega)}.
\end{aligned}
$$

Likewise, for (IMQ), we obtain

$$
\begin{aligned}
\| \hat{u}_n - u_0 \|_{L^\infty(\Omega)} &\leq \frac{N\kappa}{1-\rho} \| \mathcal{V}_n u_0 - \mathcal{V} u_0 \|_{L^\infty(\Omega)} \\
&\quad + \frac{N}{1-\rho} e^{\left(-\frac{c}{h_{\mathcal{X},\Omega}}\right)} \| u_0 \|_{\aleph_\Phi(\Omega)}.
\end{aligned}
$$

□

7 Numerical experiments

We dedicate this section to present numerical experiments. The objective is to demonstrate the effectiveness and accuracy of the proposed method in solving (1) and (2). Additionally, a comparative analysis is conducted by evaluating the performance of our approach against well-established numerical techniques. The numerical tests involve the use of three radial basis functions (RBFs): Gaussian (GA), multiquadric (MQ), and inverse multiquadric (IMQ).

To further validate the applicability of the proposed method, we compare the computational results with both the analytical solution and the MLS approach documented in [33]. The numerical implementation of the MLS method is carried out using polynomial basis functions of linear ($m = 1$), quadratic ($m = 2$), and cubic ($m = 3$) degrees, along with Gaussian weight functions. Additionally, for numerical integration, the five-point Gauss-Legendre quadrature formula is utilized.

The accuracy of the numerical approximations is quantified by evaluating the maximum and mean errors, defined as follows:

$$
\| e_n \|_2 = \left(\int_0^1 |e(t)|^2 \mathrm{d}t \right)^{\frac{1}{2}},
$$

$$
\| e_n \|_\infty = \max_{t \in [0,1]} |e(t)|,
$$

where

$$e(t) = u(t) - \hat{u}_n(t).$$

Here, $u(t)$ represents the Analytical solution, while $\hat{u}_n(t)$ corresponds to the numerical solution obtained using our proposed method.

All computations were executed on a Core(TM) i3-6006U CPU @ 2.00 GHz with 4 GB RAM. The implementation was performed using Matlab and Maple software, with a precision setting of 20 digits. The execution of all computations was performed under the default machine optimization settings without parallelization.

7.1 Class of linear FDIDEs

Example 7.1. Let be the equation:

$$\begin{cases} D^{\alpha}u(t) = f(t) + \dfrac{1}{18}u(t) + u(\theta(t)) + \displaystyle\int_0^t \frac{e^{t+s}}{4} s u(s)\mathrm{d}s + \int_0^{\theta(t)} \frac{\tau + t}{2} u(\tau)\mathrm{d}\tau, \\ u(0) = 1, \end{cases} \tag{49}$$

where $\alpha = 1$, $\theta(t) = \frac{3}{4}\sin(t)$, and the forcing term is given by

$$f(t) = \frac{(36t + 27\,\sin(t) - 36)\mathrm{e}^{-\frac{3\,\sin(t)}{4}}}{72} - \frac{t\mathrm{e}^{t}}{4} - \frac{t}{2} - \frac{19\mathrm{e}^{-t}}{18} - \frac{1}{2}.$$

For this case, the analytical solution is $u(t) = \mathrm{e}^{-t}$.

Table 1 presents the results obtained using the error metric $\|e\|_{\infty}$. According to the convergence study discussed in Remark (6.5), the numerical approximations exhibit convergence towards the analytical solution as the number of data points increases.

To further assess the performance of the proposed scheme, we tackle the Example 7.1 by employing the MLS technique and summarize the numerical outcomes in Table 2. The estimated error for the RBF method is reported in Table 3.

Table 1: Error $\|e\|_{\infty}$ for $\alpha = 1$ and $\theta(t) = \frac{3}{4}\sin(t)$ for Example 7.1 by the RBF.

	GA ($c = 2$)	IMQ ($c = 2$)
n	$\|e\|_{\infty}$	$\|e\|_{\infty}$
6	1.4×10^{-3}	1.6×10^{-4}
9	1.3×10^{-5}	1.4×10^{-6}
12	5.5×10^{-8}	1.1×10^{-8}
15	1.7×10^{-10}	7.8×10^{-11}

Table 2: $\|e\|_{\infty}$ for Example 7.1 via MLS method for $\alpha = 1$ and $\theta(t) = \frac{3}{4}\sin(t)$.

n	$m = 1$	$m = 2$	$m = 3$
4	1.2×10^{-3}	4.0×10^{-4}	1.2×10^{-4}
8	1.3×10^{-4}	3.3×10^{-5}	1.9×10^{-6}
12	7.4×10^{-6}	2.2×10^{-6}	2.3×10^{-7}
16	1.1×10^{-6}	1.5×10^{-7}	8.7×10^{-9}
20	5.3×10^{-7}	2.1×10^{-8}	2.9×10^{-9}

Figures 1 and 2 provide the results across the domain $[0, 1]$. In Figure 3, a semi-logarithmic plot compares the computational accuracy of the proposed technique against the MLS method. The high accuracy achieved by the proposed scheme is evident from these visual representations.

Furthermore, Figure 4 displays both the exact and numerically computed solutions. The computed results obtained confirm the robustness and precision of the RBF method for this class of problems.

Example 7.2. Consider the problem [11, 13]

$$\begin{cases} D^{\alpha}u(t) = f(t) - \dfrac{t^2 e^t}{5}u(t) - \dfrac{(\upsilon t)^2}{5}u(\upsilon t) + \displaystyle\int_0^t e^t s u(s)\mathrm{d}s + \int_0^{\upsilon t} \tau u(\tau)\mathrm{d}\tau, \\ u(0) = 0, \end{cases} \tag{50}$$

Table 3: RBF (MQ) error for Example 7.1.

$(\alpha = 1, \theta(t) = \frac{3}{4}\sin(t), n = 18 \text{ and } c = 2)$			
t	Analytical solution	Approximate solution	$\lvert e(t)\rvert$
0.1	0.90483741803595957	0.90483741803595846	2.72×10^{-15}
0.2	0.81873075307798185	0.81873075307796554	1.63×10^{-14}
0.3	0.74081822068171786	0.74081822068171364	4.21×10^{-15}
0.4	0.67032004603563930	0.67032004603566637	2.70×10^{-14}
0.5	0.60653065971263342	0.60653065971259149	4.19×10^{-14}
0.6	0.54881163609402643	0.54881163609405936	3.29×10^{-14}
0.7	0.49658530379140951	0.49658530379140772	1.79×10^{-15}
0.8	0.44932896411722159	0.44932896411717416	4.74×10^{-14}
0.9	0.40656965974059911	0.40656965974057963	1.94×10^{-14}
1	0.36787944117144232	0.36787944117203435	5.92×10^{-13}

in which the analytical solution is $u(t) = t^3$ and $\upsilon = \frac{1}{2}$. In this problem

$$f(t) = \begin{cases} \dfrac{6t^{2.25}}{\Gamma(3.25)}, & \text{for } \alpha = 0.75, \\ \dfrac{6t^2}{\Gamma(3)}, & \text{for } \alpha = 1. \end{cases}$$

Table 4 displays the solutions for different values of n, computed using the error norms $\|e_n\|_2$ and $\|e\|_\infty$. As predicted by the theoretical findings in Remark (6.5), increasing the number of data nodes leads to a progressive refinement of the approximations, steadily converging to the exact values.

For comparative purposes, we tackled Example 7.2 by the MLS method, with the corresponding numerical outcomes presented in Table 5. The estimated errors for the RBF approach are summarized separately in Table 6. Furthermore, Table 7 contrasts the maximum absolute error obtained by our method with that reported in [12], under the parameter settings $\upsilon = 1$ and $\alpha = 0.75$.

The error across the interval [0,1] is depicted in Figures 5 and 6, offering a visual assessment of accuracy. Additionally, the computational accuracy of Example 7.2, employing both the proposed method and the MLS approach, is illustrated in a semi-logarithmic plot in Figure 7, providing insight into precision differences between the two techniques.

To further demonstrate the effectiveness of our approach, Figure 8 presents a direct comparison between the analytical solution and the numerically estimated values. The high level of agreement observed reinforces the validity and accuracy of the RBF. The overall numerical results confirm that this approach is both efficient and reliable for solving the given problem.

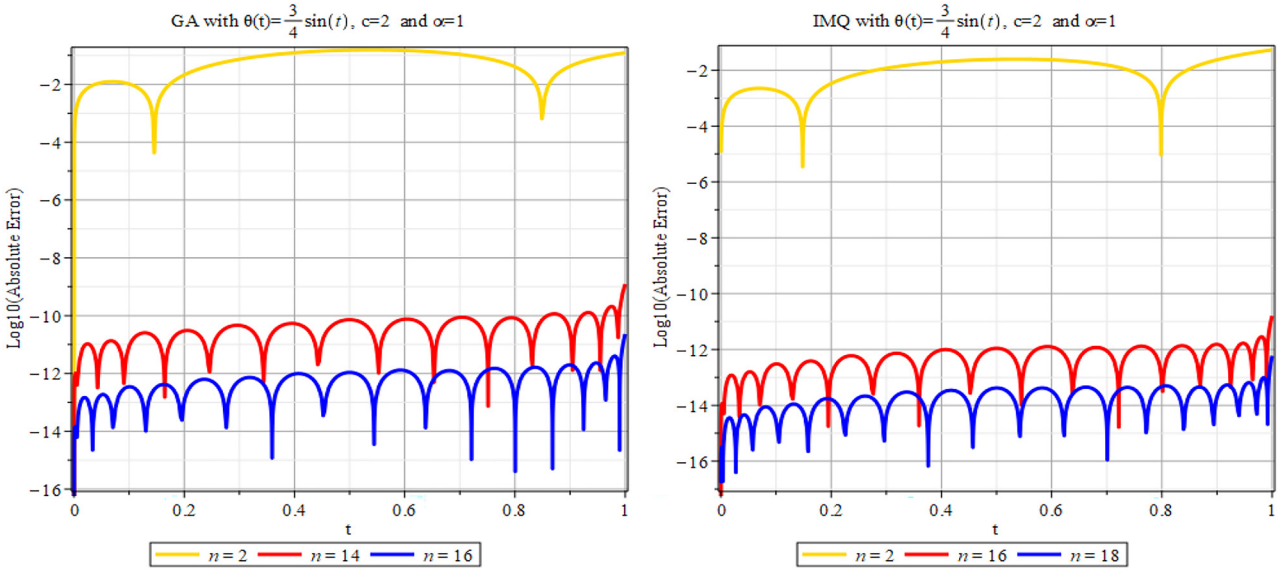


Figure 1: The error $|e(t)|$ for Example 7.1 using the proposed approach.

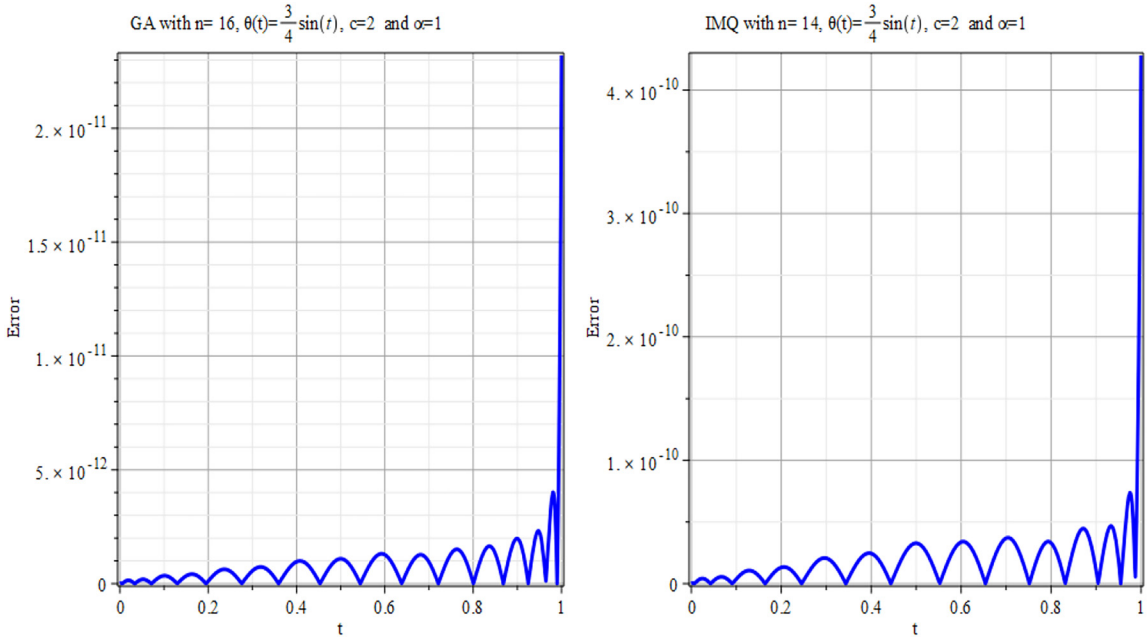


Figure 2: The absolute error for Example 7.1.

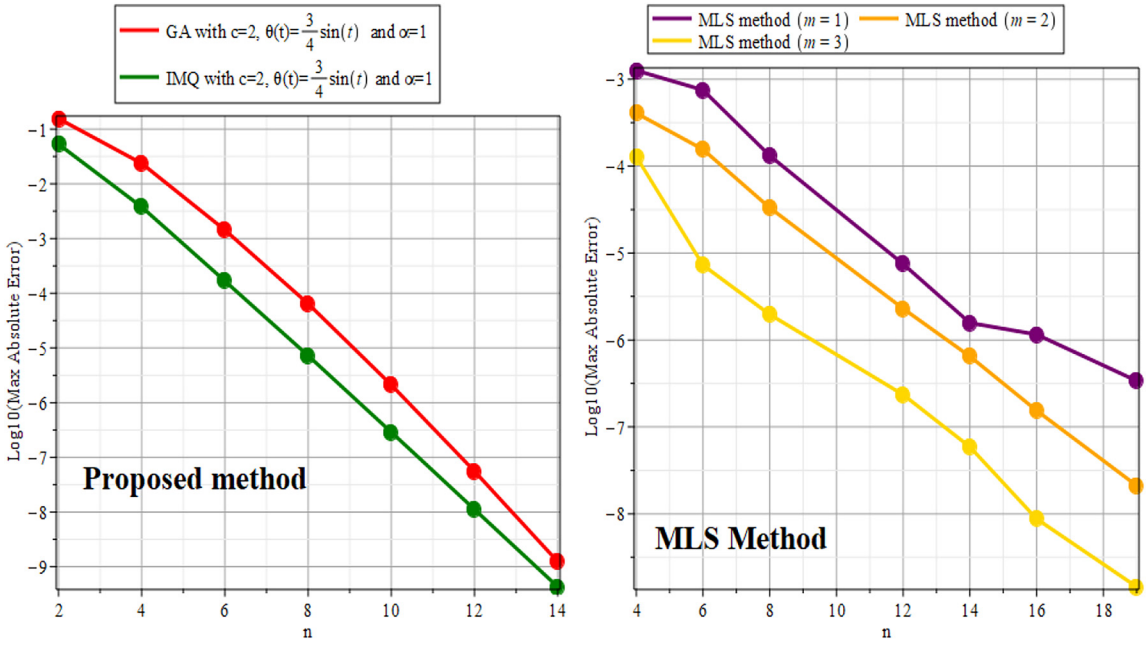


Figure 3: $|e(t)|$ for several values of n for Example 7.1 for $\alpha = 1$ and $\theta(t) = \frac{3}{4}\sin(t)$.

Example 7.3. We deal in this example with the problem reported in [34]

$$\begin{cases} D^{\alpha}u(t) = \frac{1}{2} - \frac{t}{4}e^{\frac{t}{4}} + \frac{t^2}{32} - \frac{e^{3t}}{2} + e^{2t} + \frac{1}{2}u(t) + u\left(\frac{t}{4}\right) + \int_0^t e^{t+s}u(s)\mathrm{d}s + \int_0^{\frac{t}{4}} \tau u(\tau)\mathrm{d}\tau, \\ u(0) = 0, \end{cases} \tag{51}$$

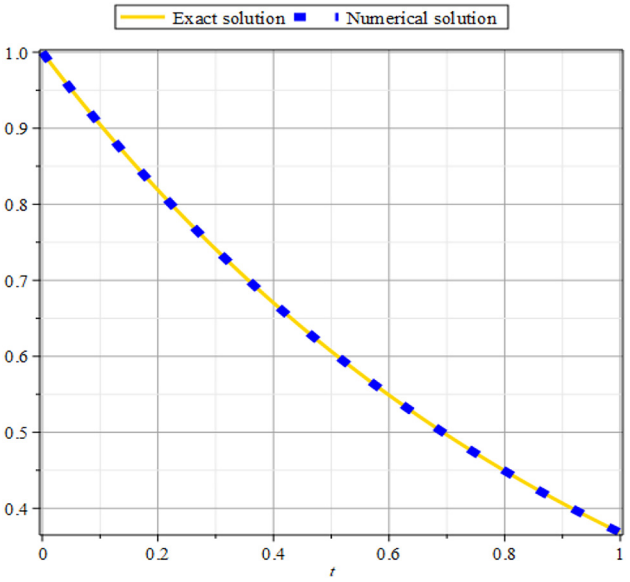


Figure 4: The analytical and RBF solutions of Example 7.1 for $\alpha = 1$ and $\theta(t) = \frac{3}{4}\sin(t)$.

For this problem, the analytical solution is $u(t) = e^t - 1$ when $\alpha = 1$.

To assess the accuracy and efficiency of the proposed methodology, numerical experiments were conducted, with errors measured using the norms $\|e_n\|_2$ and $\|e\|_\infty$ for various values of n. The corresponding results are provided in Table 8.

For comparative analysis, Example 7.3 is also solved using the MLS technique, and the numerical results for this alternative method are recorded in Table 9. Additionally, Table 10 presents a comparison of the maximum absolute error obtained by our approach against error values reported in prior studies. The estimated error associated with the RBF method is detailed separately in Table 11.

Figures 9 and 10 illustrate the absolute error distribution over the domain [0,1], providing insight into the accuracy of the numerical solutions. To further evaluate precision, Figure 11 depicts a semi-logarithmic plot comparing the computational performance of the proposed technique with that of the MLS method in solving Example 7.3.

Table 5: $\|e\|_\infty$ for Example 7.2 via MLS method for $\alpha = 1$ and $\upsilon = \frac{1}{2}$.

n	$m = 1$	$m = 2$
4	1.3×10^{-2}	5.2×10^{-3}
8	1.4×10^{-3}	3.3×10^{-4}
12	7.3×10^{-5}	2.3×10^{-5}
16	7.0×10^{-6}	1.6×10^{-6}
20	1.7×10^{-6}	2.6×10^{-7}

Table 6: The RBF (MQ) error for Example 7.2.

	$(\alpha = 1, \upsilon = \frac{1}{2}, n =$ and $c = 2)$		
t	Analytical solution	Approximate solution	$\lvert e(t)\rvert$
0.1	0.001000000000	0.00100000000047	4.77×10^{-13}
0.2	0.008000000000	0.00799999999947	5.23×10^{-13}
0.3	0.027000000000	0.02700000000029	2.99×10^{-13}
0.4	0.064000000000	0.06399999999994	5.15×10^{-14}
0.5	0.125000000000	0.12500000000012	1.20×10^{-13}
0.6	0.216000000000	0.21599999999995	4.39×10^{-14}
0.7	0.343000000000	0.34300000000021	2.11×10^{-13}
0.8	0.512000000000	0.51199999999940	5.98×10^{-13}
0.9	0.729000000000	0.72900000000115	1.15×10^{-12}
1	1	0.99999999997110	2.88×10^{-11}

Finally, Figure 12 presents a direct comparison between the analytical solution and the numerical approximation. The close agreement between these solutions underscores the reliability and effectiveness of the proposed approach. Overall, the numerical findings reinforce that this methodology offers both high precision and computational efficiency for solving the given problem.

Example 7.4. This example is from [34]

$$\begin{cases} D^{\alpha}u(t) = u(t) - \frac{1}{2}\ln\left(1+\frac{t}{2}\right)u\left(\frac{t}{2}\right) + \frac{1}{1+t} - \ln(1+t)\left(\frac{t}{2}\ln(1+t)+1\right) \\ + \int_0^t \frac{t}{1+s}u(s)\mathrm{d}s + \int_0^{\frac{t}{2}} \frac{1}{1+s}u(s)\mathrm{d}s, \\ u(0) = 0, \end{cases} \tag{52}$$

Table 4: Estimated errors $\|e\|_2$ and $\|e\|_\infty$ for $\alpha = 1$ and $\upsilon = \frac{1}{2}$ for Example 7.2 by applying the current methodology.

	Gaussians ($c = 2$)	Gaussians ($c = 2$)	Inverse multiquadrics ($c = 2$)	Inverse multiquadrics ($c = 2$)	Multiquadrics ($c = 2$)
n	$\|e\|_\infty$	$\|e\|_2$	$\|e\|_\infty$	$\|e\|_2$	$\|e\|_\infty$
5	1.6×10^{-2}	2.5×10^{-3}	2.6×10^{-3}	3.8×10^{-4}	8.0×10^{-4}
10	8.2×10^{-6}	7.2×10^{-7}	1.6×10^{-6}	1.4×10^{-7}	5.5×10^{-7}
15	4.9×10^{-10}	3.0×10^{-11}	2.1×10^{-10}	1.2×10^{-11}	2.8×10^{-11}

Table 7: The absolute error for Example 7.2 with $\alpha = 0.75$ and $\upsilon = 1$.

J	N	Ref [12] ($E_c(N)$)	n	Our method (inverse multiquadrics (c = 7))	Our method (multiquadrics (c = 7))
1	4	7.10×10^{-3}	4	4.75×10^{-3}	3.05×10^{-3}

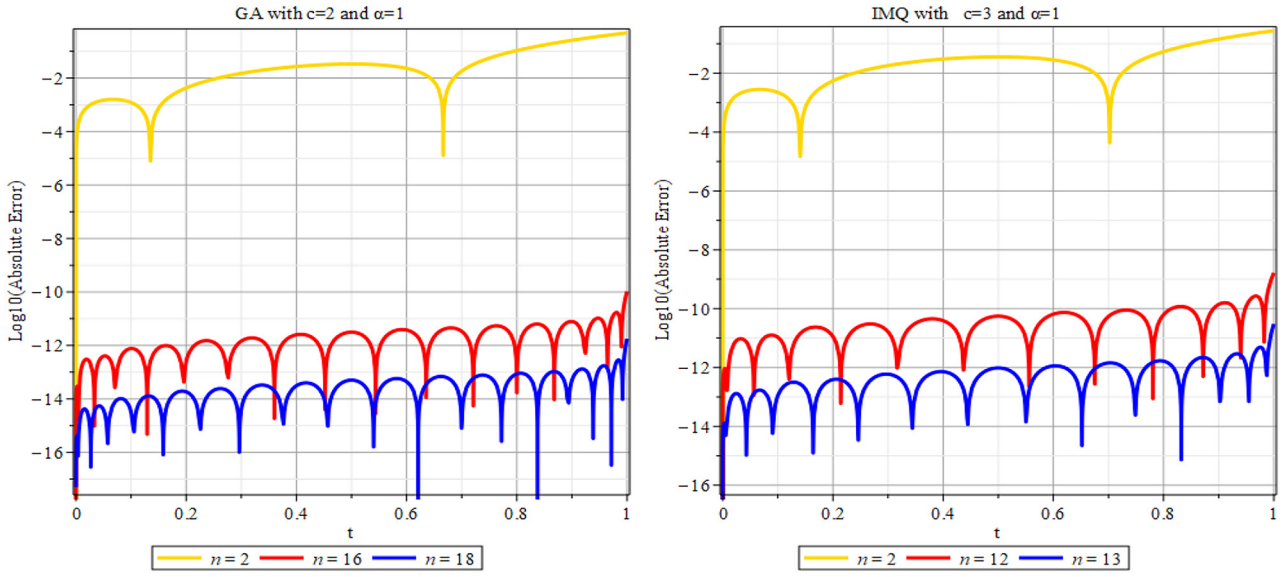


Figure 5: The error $|e(t)|$ for Example 7.2 using the proposed approach.

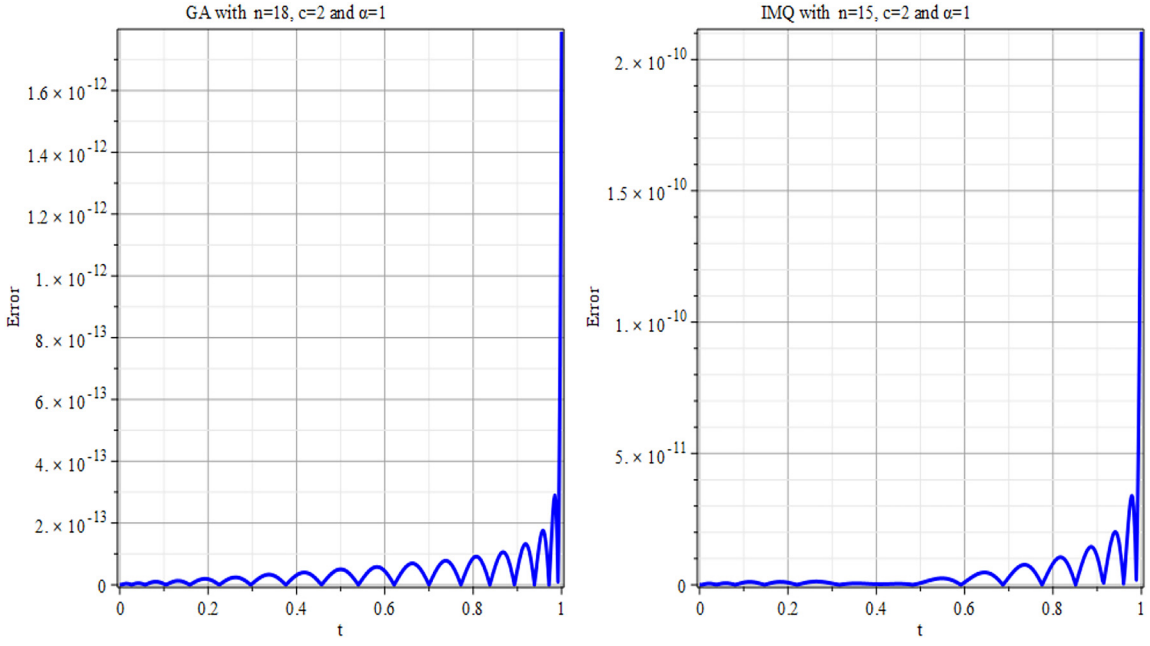


Figure 6: Absolute error of Example 7.2.

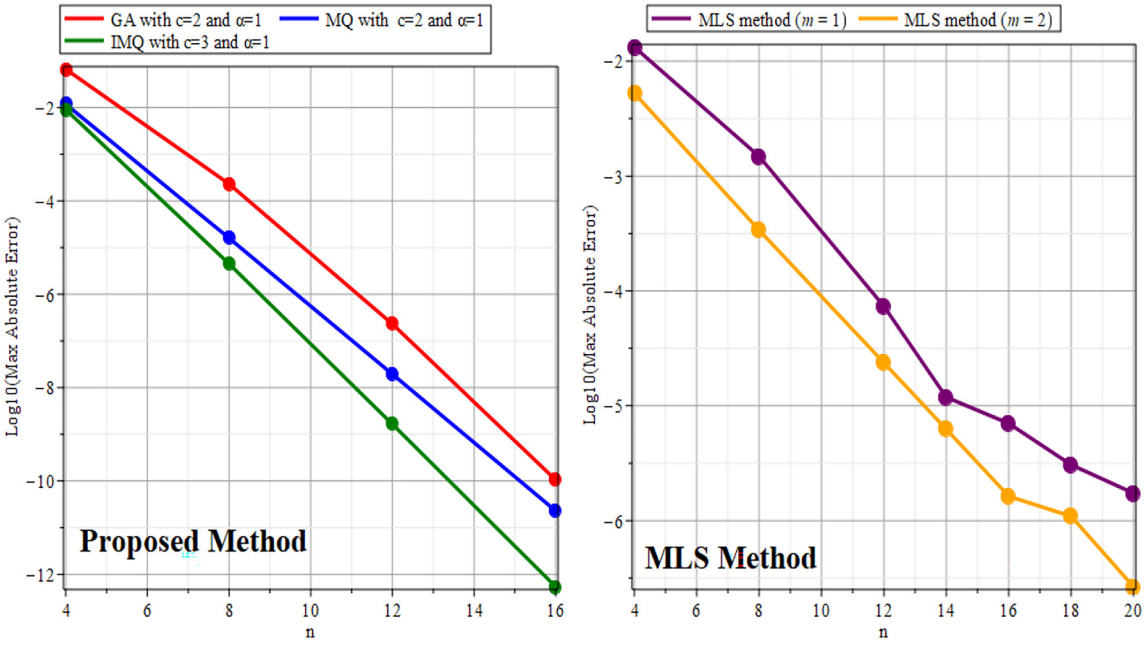


Figure 7: $|e(t)|$ for $\alpha = 1$ and for snumerous numbers of n for Example 7.2.

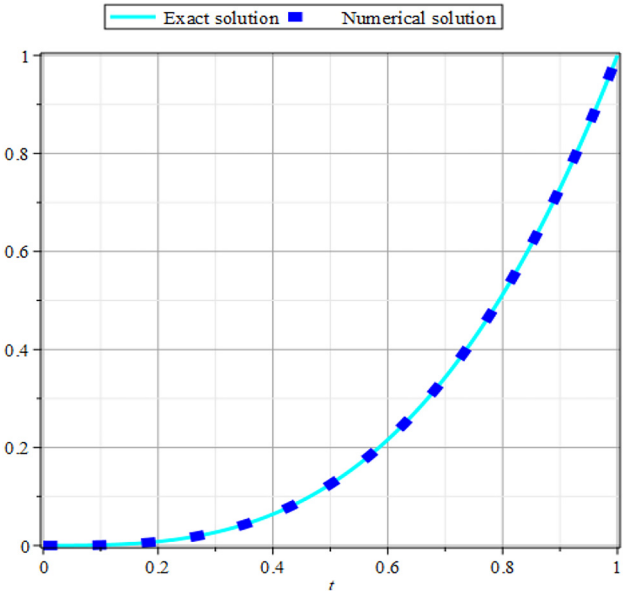


Figure 8: The analytical and RBF solutions of Example 7.2 for $\alpha = 1$.

The analytical solution in this case is $u(t) = \ln(1+t)$ when $\alpha = 1$. Table 12 showcases the solutions computed using the error norm $\|e_n\|_\infty$.

To facilitate a comparative analysis, Example 7.4 is also solved utilizing the MLS technique, with the corresponding numerical findings summarized in Table 13. Furthermore, Table 14 provides a comparative assessment of the maximum absolute error obtained by our approach against those reported for alternative techniques in the existing literature. The estimated errors associated with the RBF method are compiled in Table 15.

The absolute error function across the domain [0,1] is graphically represented in Figures 13 and 14, offering a visual insight into the error behavior. Additionally, Figure 15 illustrates the computational accuracy of Example 7.4 by comparing the performance of the proposed methodology with the MLS approach, presented in a semi-logarithmic format.

Lastly, Figure 16 depicts a direct comparison between the analytical solution and the numerical approximation, highlighting the high degree of accuracy achieved by the suggested technique. The results obtained for this class of problems affirm the effectiveness and precision of the proposed approach.

7.2 Class of nonlinear FDIDEs

Example 7.5. Consider the problem

$$\begin{cases} D^{\alpha}u(t) = f(t) + u(\theta(t)) + \int_0^t K_1(t,s)G_1(u(s))\mathrm{d}s + \int_0^{\theta(t)} K_2(t,\tau)G_2(u(\tau))\mathrm{d}\tau, \\ u(0) = 1, \end{cases} \tag{53}$$

in which $\alpha = 1$, $\theta(t) = \frac{3}{5}t$, $G_1(u) = e^u$, $G_2(u) = u^2$, $K_1(t,s) = t$, $K_2(t,\tau) = t\tau$, $f(t) = -\frac{\mathrm{erfi}(t^2)\sqrt{\pi}t}{4} - \frac{2187\left(t^7 + \frac{3125}{27}t - \frac{7812500}{2187}\right)t^3}{1953125}$ and the analytical solution is $u(t) = t^4$.

Table 8: Error $\|e\|_\infty$ for Example 7.3 using the proposed approach.

	Gaussians ($c = 2$)	Gaussians ($c = 2$)	Inverse multiquadrics ($c = 3$)	Multiquadrics($c = 2$)
n	$\|e\|_2$	$\|e\|_\infty$	$\|e\|_\infty$	$\|e\|_\infty$
3	3.2×10^{-2}	1.5×10^{-1}	2.1×10^{-2}	1.8×10^{-2}
5	1.9×10^{-3}	1.3×10^{-2}	5.8×10^{-4}	7.2×10^{-4}
7	8.0×10^{-5}	6.9×10^{-4}	1.3×10^{-5}	2.6×10^{-5}
9	2.5×10^{-6}	2.6×10^{-5}	2.7×10^{-7}	9.7×10^{-7}
11	6.4×10^{-8}	7.9×10^{-7}	5.6×10^{-9}	3.5×10^{-8}

Table 9: $\|e\|_\infty$ for Example 7.3 with several values of m, n using MLS method.

n	$m = 1$	$m = 2$	$m = 3$
5	8.0×10^{-3}	1.9×10^{-4}	1.8×10^{-4}
10	1.9×10^{-5}	1.5×10^{-5}	1.5×10^{-6}
15	8.6×10^{-6}	5.4×10^{-7}	5.6×10^{-8}

Table 16 presents the numerical results obtained for various values of n, evaluated using the norm $\|e\|_\infty$. These values provide insight into the accuracy and convergence behavior of the proposed approach.

To further analyze the error characteristics, Table 17 displays the estimated errors associated with the RBF method. Additionally, Figures 17 and 18 illustrate the absolute error distribution across the interval [0,1], visually demonstrating how the error evolves over the domain.

For a comparative assessment of computational precision, Figure 19 presents a semi-logarithmic plot that juxtaposes the performance of the outlined technique with the MLS method in solving Example 7.5. The graphical representation highlights the numerical stability and efficiency of the proposed scheme.

Moreover, Figure 20 provides a direct comparison between the analytical solution and the numerically computed approximation, further reinforcing the accuracy of the methodology.

Overall, the numerical findings presented here validate the reliability and effectiveness of the proposed approach for addressing this class of problems. The high degree of precision observed across the tests confirms that the method is not only computationally efficient but also robust in delivering accurate solutions.

Table 11: Estimate of RBF error (IMQ) for Example 7.3.

	($\alpha = 1$, $n = 13$, and $c = 5$)		
T	Analytical solution	Approximate solution	$\|e(t)\|$
0.1	0.10517091807564	0.105170918075714	6.63×10^{-14}
0.2	0.22140275816016	0.221402758160192	2.21×10^{-14}
0.3	0.34985880757600	0.349858807576051	4.78×10^{-14}
0.4	0.49182469764127	0.491824697641339	6.86×10^{-14}
0.5	0.64872127070012	0.648721270700172	4.38×10^{-14}
0.6	0.82211880039050	0.822118800390534	2.50×10^{-14}
0.7	1.01375270747047	1.013752707470560	8.34×10^{-14}
0.8	1.22554092849246	1.225540928492570	1.02×10^{-13}
0.9	1.45960311115694	1.459603111157017	6.73×10^{-14}
1	1.71828182845904	1.718281828458312	7.33×10^{-13}

Example 7.6. Consider the problem

$$\begin{cases} D^\alpha u(t) = f(t) + u(\theta(t)) + \int_0^t K_1(t,s)G_1(u(s))\mathrm{d}s + \int_0^{\theta(t)} K_2(t,\tau)G_2(u(\tau))\mathrm{d}\tau, \\ u(0) = 1, \end{cases} \tag{54}$$

in which $\alpha = \frac{1}{10}$, $\theta(t) = \frac{1}{5}\arctan(t)$, $G_1(u) = u^2$, $G_2(u) = u^2$, $K_1(t,s) = \sin(s)$, $K_2(t,\tau) = t\tau$, and $f(t)$ is defined such that the analytical solution is $u(t) = t^3$.

Table 10: MAE error for Example 7.3.

N	Ref [35]MAEs	M	Ref [36]MAEs	m	Ref [37]MAEs	M	Ref [34]MAEs	n	Our approach (MQ) ($c = 7$)
20	5.72×10^{-6}	6	1.68×10^{-7}	5	2.63×10^{-6}	10	4.50×10^{-10}	10	1.21×10^{-11}
40	2.20×10^{-8}	8	1.10×10^{-10}	6	1.94×10^{-6}	12	1.42×10^{-10}	11	6.27×10^{-12}

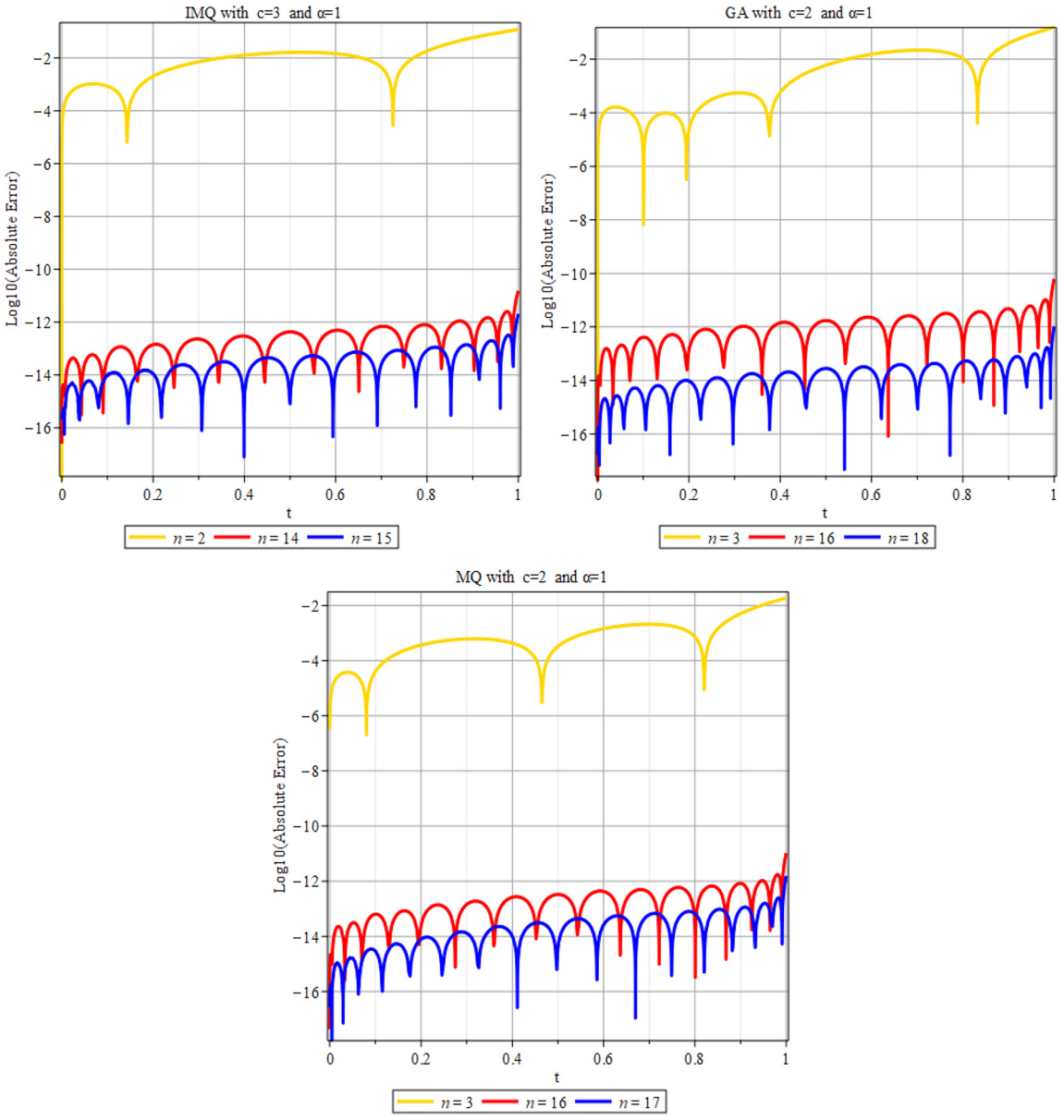


Figure 9: The error $|e(t)|$ for Example 7.3 using the proposed approach.

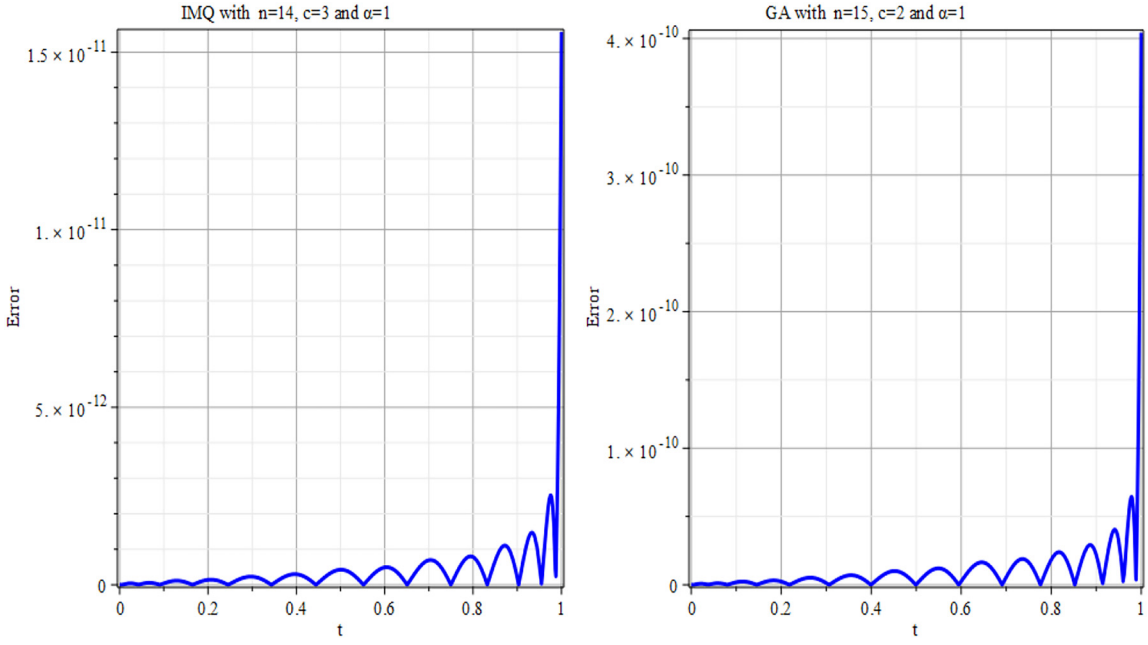


Figure 10: Absolute error of Example 7.3.

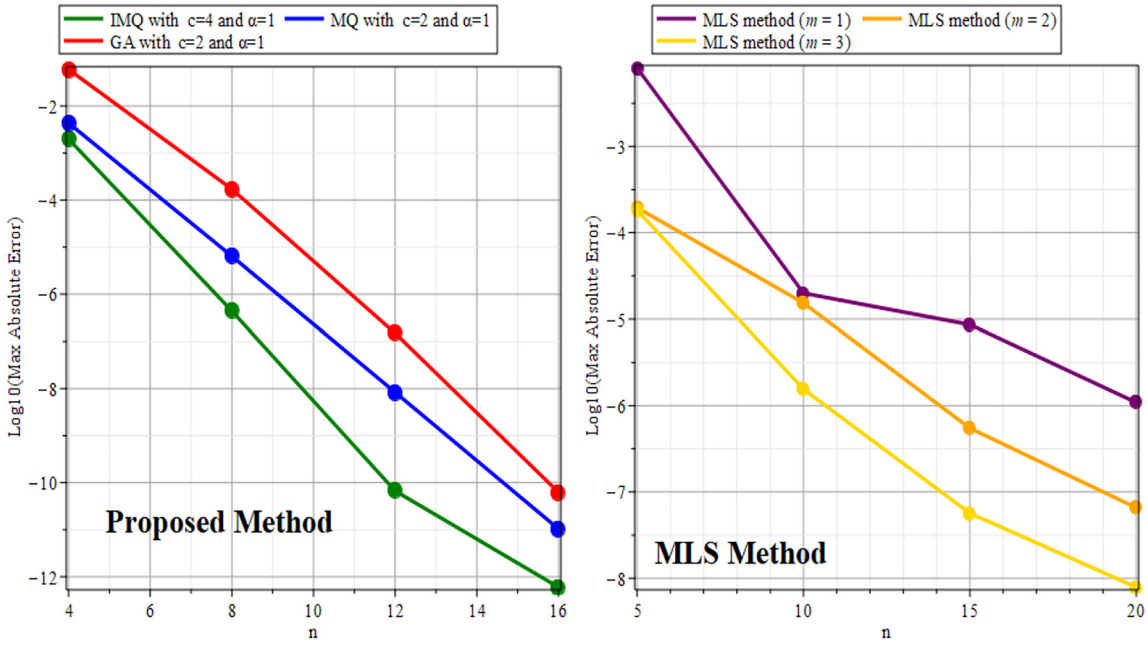


Figure 11: $|e(t)|$ for $\alpha = 1$ and for multiple selections of n for Example 7.3.

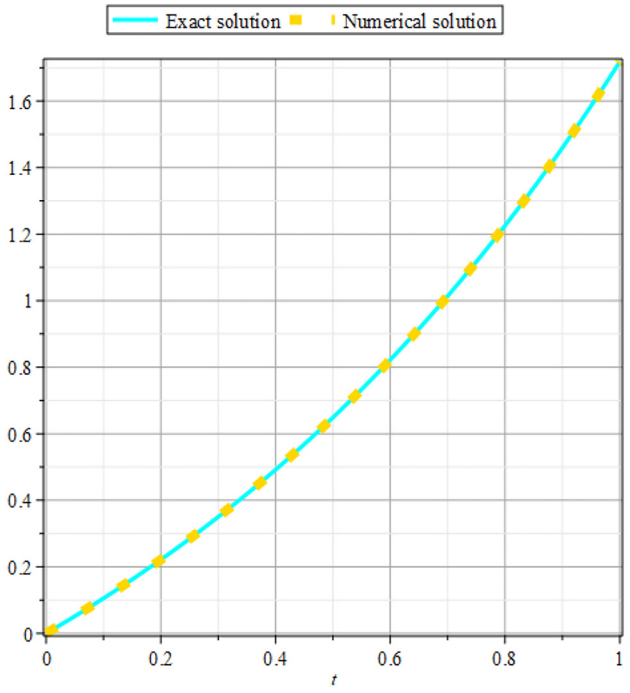


Figure 12: The analytical and RBF solution of Example 7.3.

Table 12: Error $\|e\|_\infty$ for Example 7.4 using the proposed approach.

	Gaussians ($c = 2$)	Multiquadrics ($c = 2$)	Inverse multiquadrics($c = 3$)
n	$\|e\|_\infty$	$\|e\|_\infty$	$\|e\|_\infty$
4	2.3×10^{-2}	2.0×10^{-3}	1.8×10^{-3}
8	7.4×10^{-5}	6.4×10^{-6}	3.1×10^{-6}
12	8.5×10^{-8}	1.8×10^{-8}	4.9×10^{-9}
16	6.3×10^{-11}	5.1×10^{-11}	7.9×10^{-12}

Table 13: $\|e\|_\infty$ for Example 7.4 with several values of m, n using MLS method.

n	$m = 1$	$m = 2$	$m = 3$
5	2.1×10^{-3}	1.7×10^{-5}	1.7×10^{-5}
10	5.5×10^{-6}	4.7×10^{-6}	3.3×10^{-6}
15	2.1×10^{-6}	2.0×10^{-7}	1.7×10^{-8}
20	4.1×10^{-7}	2.4×10^{-8}	6.1×10^{-9}

Table 15: Estimate of RBF error (GA) of Example 7.4.

($\alpha = 1$, $n = 20$ and $c = 2$)			
t	Analytical solution	Approximate solution	$\|e(t)\|$
0.1	0.09531017980432	0.0953101798043255	6.39×10^{-16}
0.2	0.18232155679395	0.1823215567939541	5.26×10^{-16}
0.3	0.26236426446749	0.2623642644674941	3.04×10^{-15}
0.4	0.33647223662129	0.3364722366212150	2.06×10^{-15}
0.5	0.40546510810816	0.4054651081081617	2.68×10^{-15}
0.6	0.47000362924573	0.4700036292457388	3.24×10^{-15}
0.7	0.53062825106217	0.5306282510621801	9.70×10^{-15}
0.8	0.58778666490211	0.5877866649021242	5.19×10^{-15}
0.9	0.64185388617239	0.6418538861723981	3.32×10^{-15}
1	0.69314718055994	0.6931471805599073	3.80×10^{-14}

Table 18 presents the numerical results obtained for various values of n, evaluated using the error norm $\|e\|_\infty$. These results offer valuable insights into the accuracy and convergence of the proposed method as the number of data points increases.

To further assess the error behavior, Table 19 provides the estimated errors associated with the RBF approach, offering a quantitative measure of the approximation quality. Additionally, Figure 21 illustrates the computational precision of Example 7.6, comparing the performance of the proposed technique with that of the MLS method in a semi-logarithmic format. This comparison underscores the numerical stability and effectiveness of the outlined methodology.

Furthermore, Figure 22 visually contrasts the analytical solution with the estimated numerical approximation. The high degree of agreement between these solutions further validates the effectiveness of the method.

Overall, the numerical findings presented here confirm the robustness, reliability, and precision of the proposed technique in solving this class of problems. The accuracy observed across the computational experiments highlights the method's efficiency and its suitability for obtaining highly precise numerical solutions.

Table 14: The comparative evaluation of the greatest absolute error for the Example 7.4.

M	Ref [35]MAEs	M	Ref [34]MAEs	n	Our method(IMQ (c = 6))	Our method(MQ (c = 6))
10	1.11×10^{-4}	10	5.17×10^{-8}	10	3.29×10^{-8}	3.04×10^{-8}
40	6.26×10^{-9}	12	2.50×10^{-9}	12	1.09×10^{-9}	8.39×10^{-10}

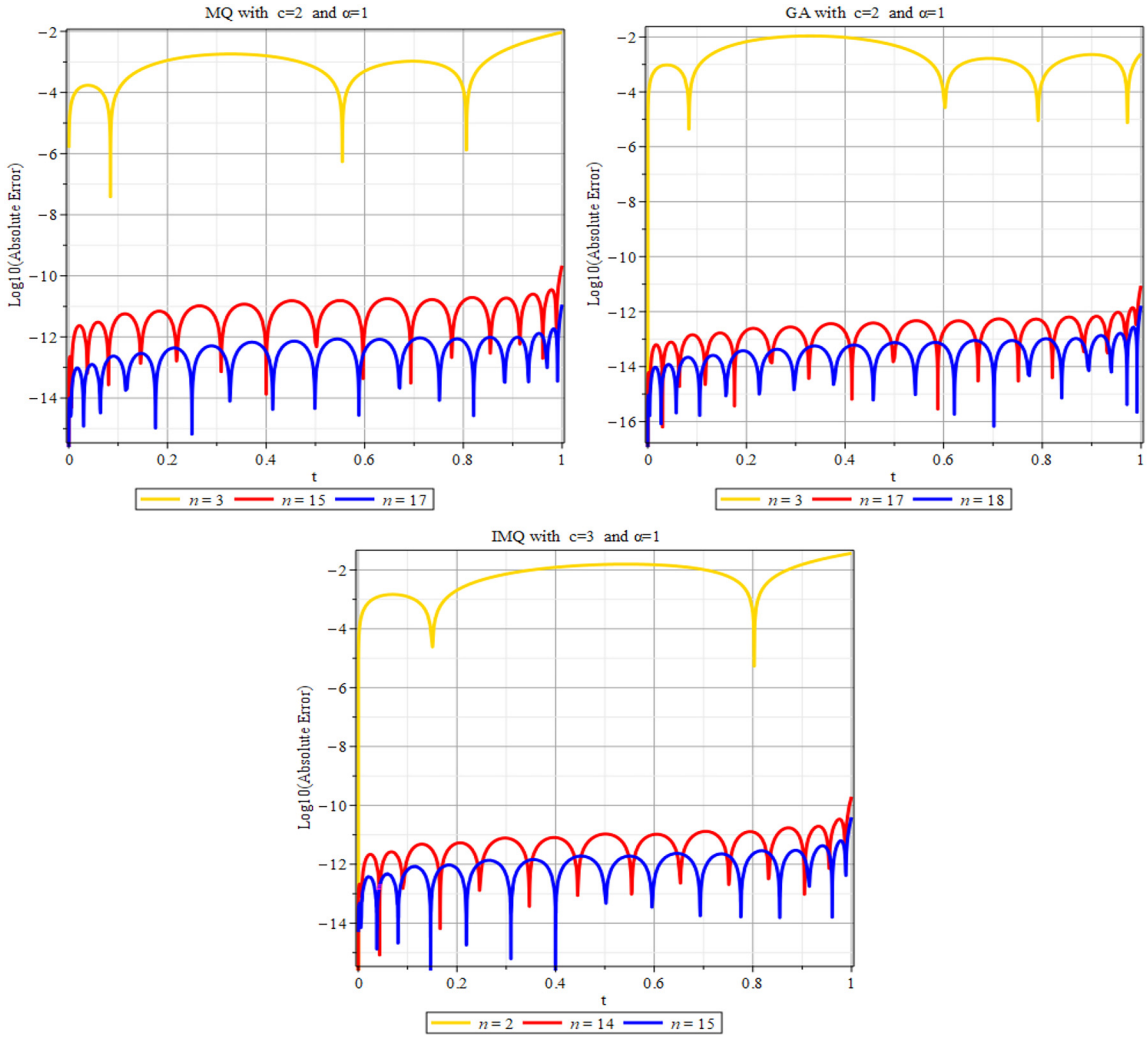


Figure 13: The error $|e(t)|$ for Example 7.4 using the proposed approach.

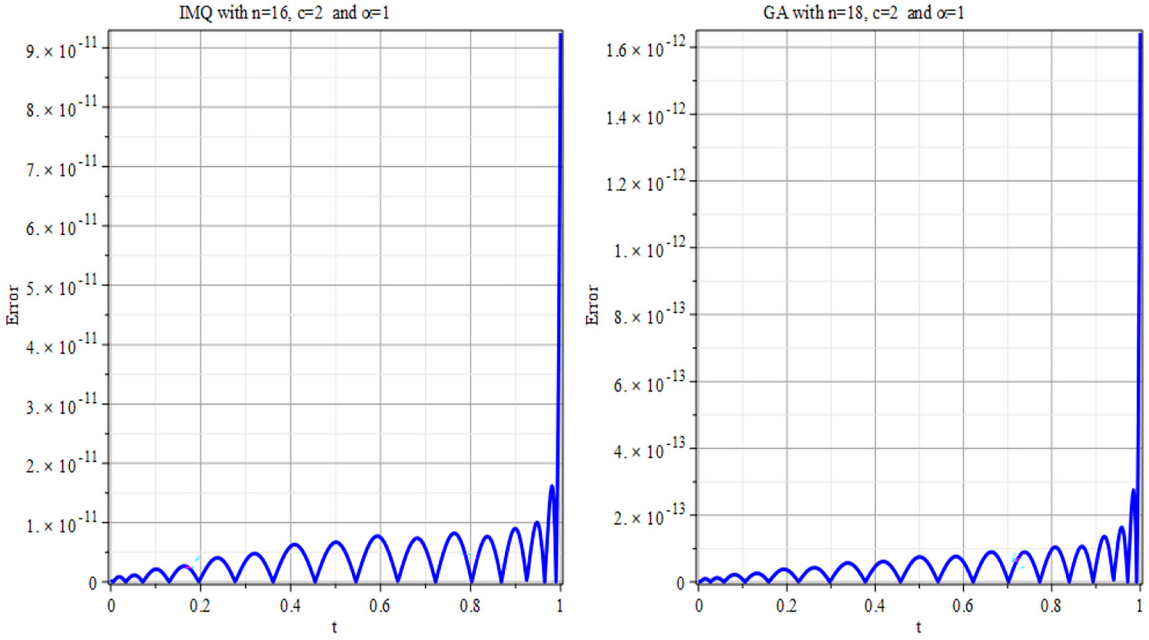


Figure 14: The absolute error for Example 7.4.

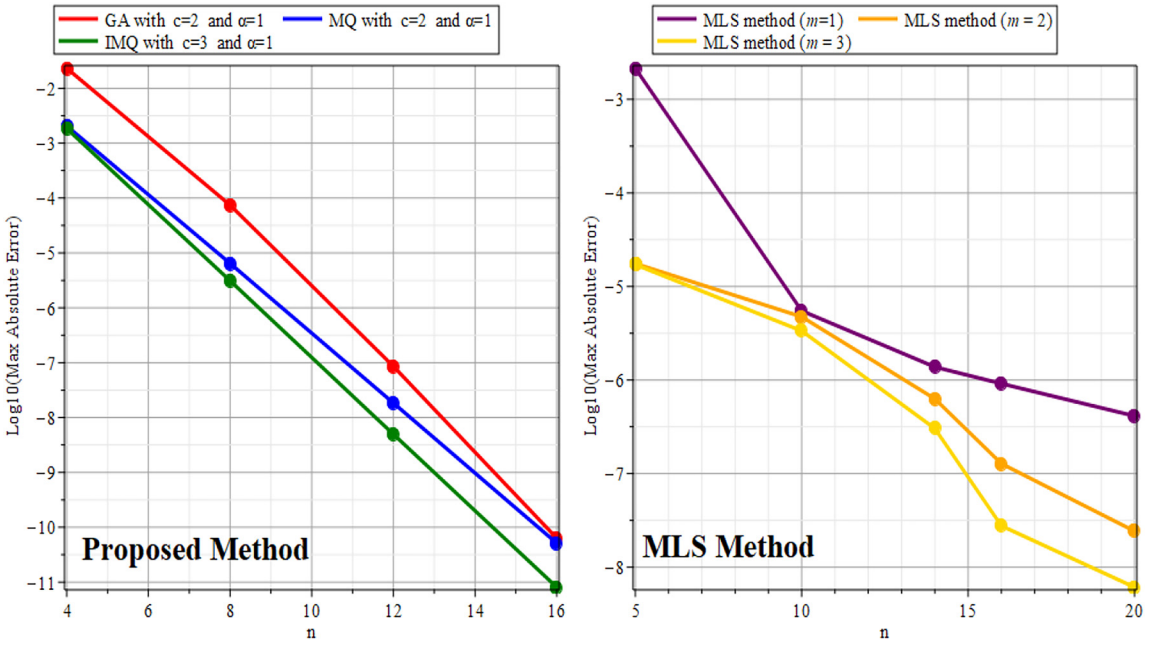


Figure 15: $|e(t)|$ for several values of n for Example 7.4.

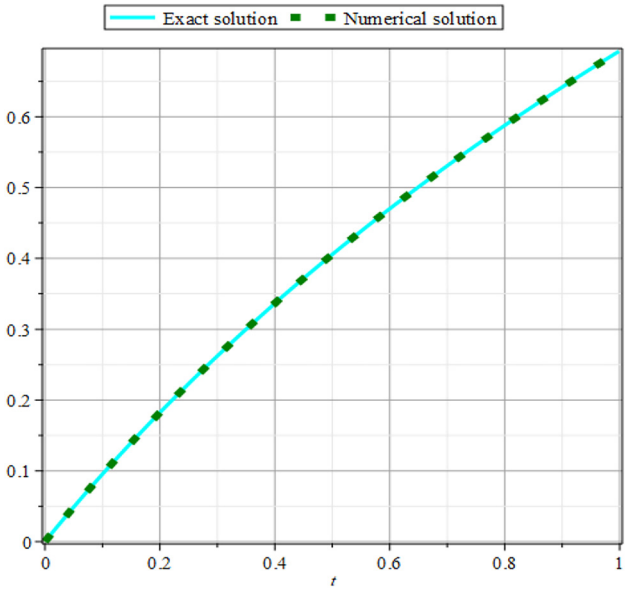


Figure 16: The analytical and RBF solution of Example 7.4.

Table 17: RBF error estimate (MQ) of Example 7.5.

$(\alpha = 1, \theta(t) = \frac{3}{5}t, n = 15 \text{ and } c = 2)$			
t	**Analytical solution**	**Approximate solution**	$\lvert e(t)\rvert$
0.1	0.0001000000000000	0.000099999991890	8.10×10^{-12}
0.2	0.0016000000000000	0.001600000010276	1.02×10^{-11}
0.3	0.0081000000000000	0.008099999994418	5.58×10^{-12}
0.4	0.0256000000000000	0.025599999999051	9.48×10^{-13}
0.5	0.0625000000000000	0.062500000001458	1.45×10^{-12}
0.6	0.1296000000000000	0.129599999991125	8.87×10^{-12}
0.7	0.2401000000000000	0.240100000025167	2.51×10^{-11}
0.8	0.4096000000000000	0.409599999928336	7.16×10^{-11}
0.9	0.6561000000000000	0.656100000077385	7.73×10^{-11}
1	1	0.999999998695804	1.30×10^{-9}

Table 16: Errors $\|e\|_\infty$ and $\|e\|_2$ for $\alpha = \frac{1}{10}$ and $\alpha = 1$ and $\theta(t) = \frac{3}{5}t$ for Example 7.5 using the proposed approach.

	IMQ ($c = 2$)	**IMQ ($c = 2$)**	**GA ($c = 2$)**	**GA ($c = 2$)**
n	$\|e\|_\infty$	$\|e\|_2$	$\|e\|_\infty$	$\|e\|_2$
4	3.5×10^{-2}	6.1×10^{-3}	9.9×10^{-2}	1.7×10^{-2}
8	7.5×10^{-5}	7.7×10^{-6}	3.8×10^{-4}	3.9×10^{-5}
12	1.1×10^{-7}	8.8×10^{-8}	3.9×10^{-7}	2.9×10^{-8}
15	1.3×10^{-9}	8.4×10^{-11}	1.7×10^{-9}	1.0×10^{-10}

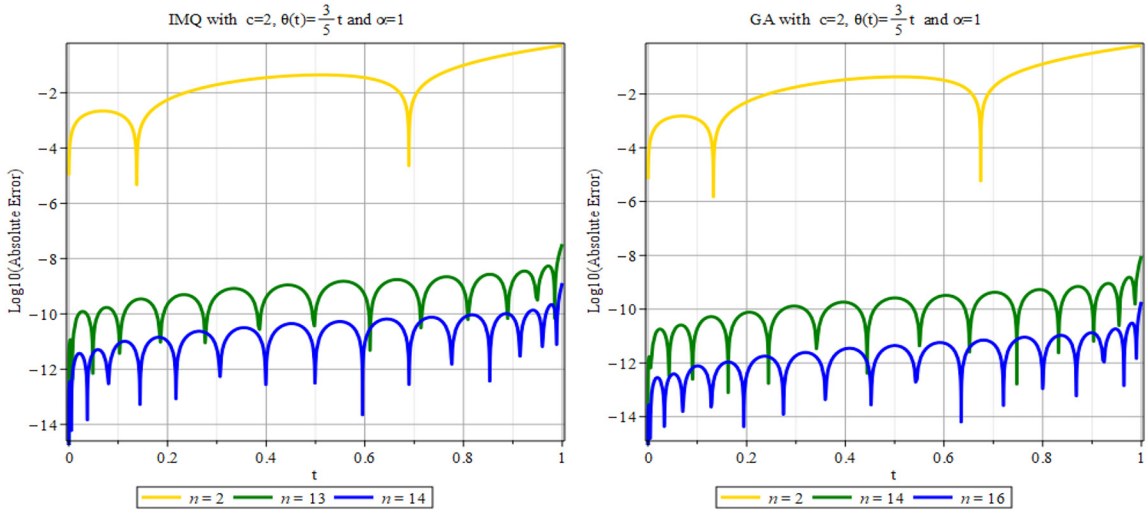


Figure 17: The error $|e(t)|$ for Example 7.5 using the proposed approach.

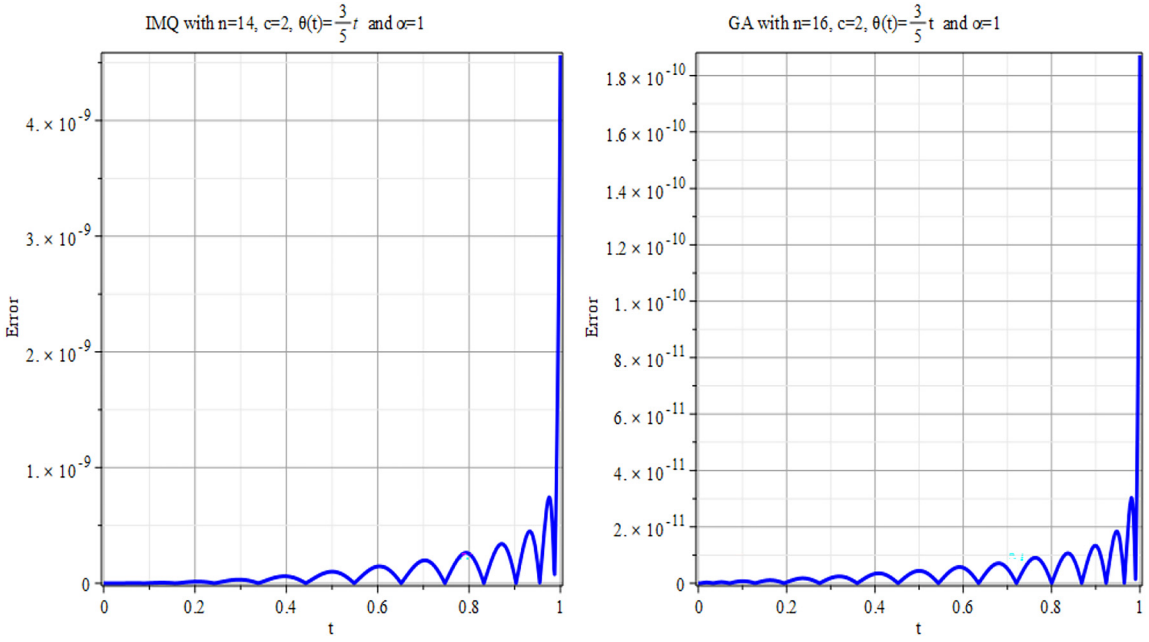


Figure 18: The absolute error for Example 7.5.

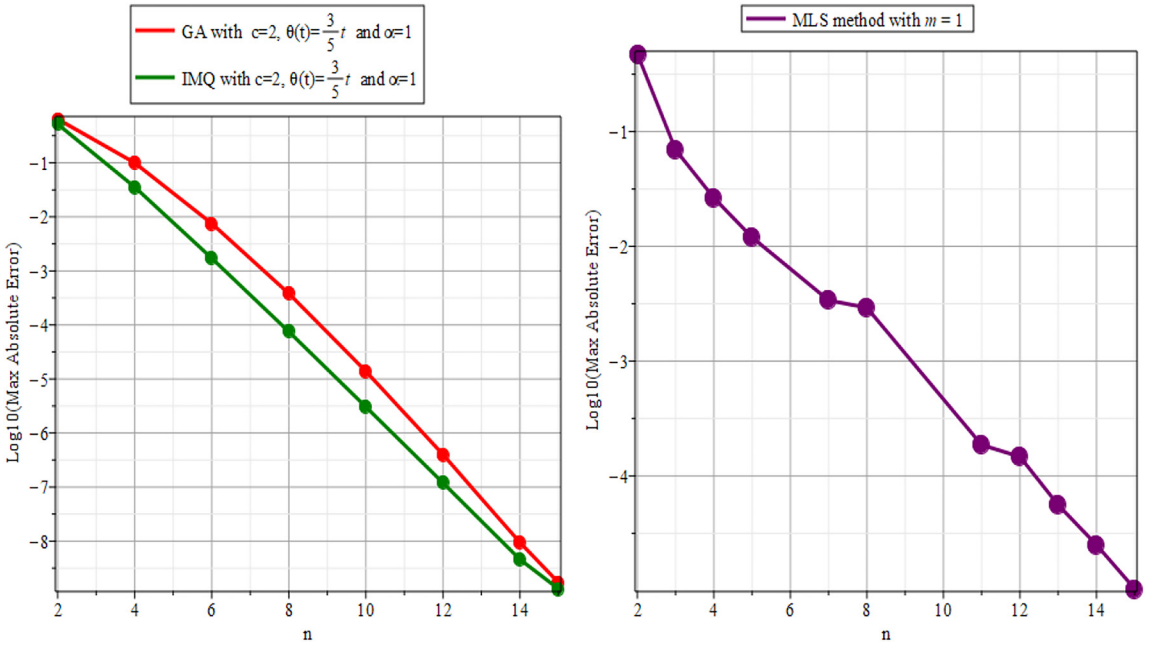


Figure 19: $|e(t)|$ for a number of selected values of n for Example 7.5 for $\alpha = 1$ and $\theta(t) = \frac{3}{5}t$.

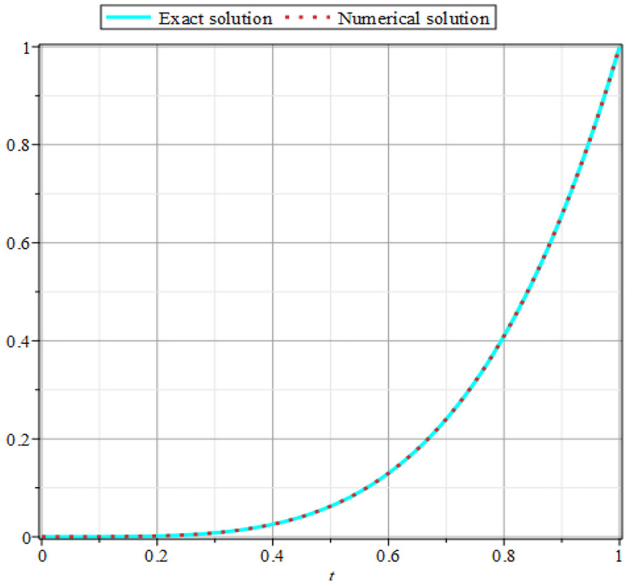


Figure 20: The RBF and analytical solution of Example 7.5 for $\alpha = 1$ and $\theta(t) = \frac{3}{5}t$.

Table 18: Error $\|e\|_\infty$ for $\alpha = \frac{1}{10}$ and $\theta(t) = \frac{1}{5}\arctan(t)$ for Example 7.6 by applying the suggested methodology.

	GA ($c = 2$)	IMQ ($c = 2$)
n	$\|e\|_\infty$	$\|e\|_\infty$
5	3.4×10^{-2}	3.2×10^{-3}
8	8.1×10^{-4}	1.9×10^{-4}
11	2.0×10^{-5}	1.6×10^{-5}
14	6.8×10^{-6}	6.5×10^{-6}

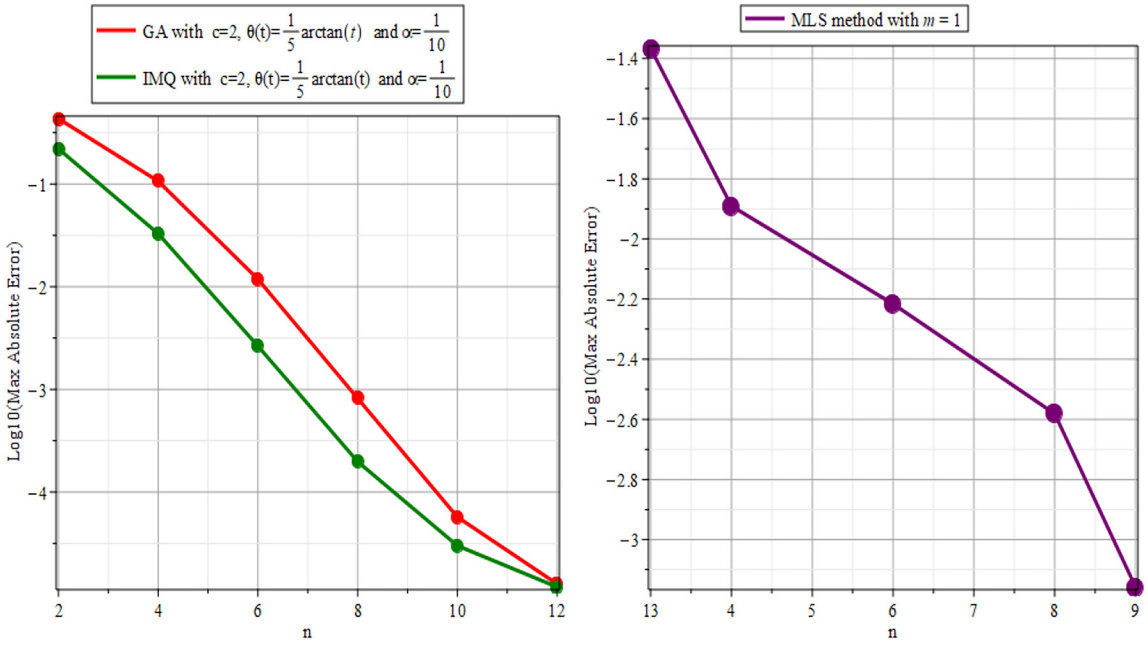


Figure 21: $|e(t)|$ for a number of selected values of n for Example 7.6 for $\alpha = \frac{1}{10}$ and $\theta(t) = \frac{1}{5}\arctan(t)$.

Table 19: RBF (GA) error estimation for Example 7.6.

$(\alpha = \frac{1}{10}, \theta(t) = \frac{1}{5}\arctan(t), n = 15 \text{ and } c = 2)$			
t	Analytical solution	Approximate solution	$\lvert e(t)\rvert$
0.1	0.00100000000	0.00099999575	4.24×10^{-9}
0.2	0.00800000000	0.00799996602	3.39×10^{-8}
0.3	0.02700000000	0.02699988529	1.14×10^{-7}
0.4	0.06400000000	0.06399972775	2.72×10^{-7}
0.5	0.12500000000	0.12499946638	5.33×10^{-7}
0.6	0.21600000000	0.21599907029	9.29×10^{-7}
0.7	0.34300000000	0.34299849965	1.50×10^{-6}
0.8	0.51200000000	0.51199769545	2.30×10^{-6}
0.9	0.72900000000	0.72899656174	3.43×10^{-6}
1	1	0.99999492898	5.07×10^{-6}

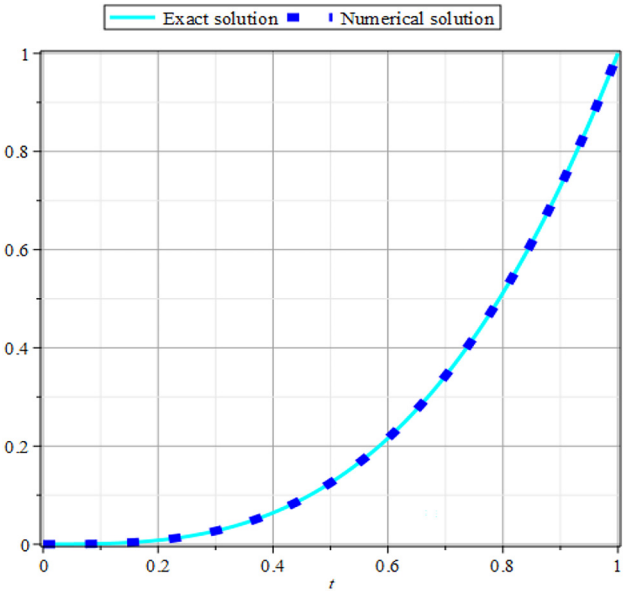


Figure 22: The RBF and analytical solution of Example 7.6 for $\alpha = \frac{1}{10}$ and $\theta(t) = \frac{1}{5}\arctan(t)$.

8 Conclusions

This paper has presented an efficient computational methodology to address fractional delay-integro-differential equations (FDIDEs) characterized by vanishing variable delays. Using radial basis function (RBF) approximations over scattered points, we established a collocation framework that does not require an underlying mesh structure. This feature thereby offers a flexible and mesh-free approach to numerical problem-solving. The Gauss-Legendre integration rule was used to discretize the integral components within the equations. A rigorous error analysis was conducted. After numerical tests, the developed scheme has a strong convergence rate. Particularly, we tested it on various numerical examples, all of which demonstrated high accuracy and efficiency. Furthermore, comparative assessments with the MLS collocation method reaffirmed the superior precision and reduced computational complexity of our proposed scheme.

Despite its efficiency, the methodology has some inherent challenges. A significant limitation of the RBF-based approach is its sensitivity to the selection of the shape parameter. This choice has a direct impact on both accuracy and stability. Identifying an optimal shape parameter remains an open problem that requires further exploration. Additionally, while the scheme exhibits robustness for problems involving vanishing variable delays, its performance when applied to delay functions with abrupt changes or discontinuities remains to be fully examined. Another potential drawback is the computational complexity of high-dimensional cases. Such case may need adaptive strategies or domain decomposition techniques to maintain efficiency. To advance this research, one can explore more research directions. In fact, future efforts could focus on developing automated or data-driven methods for optimal shape parameters. This perspective can improve accuracy and stability. Furthermore, extending the current framework to handle FDIDEs with complex boundary conditions or irregular domains would further enhance its applicability. Additionally, integrating machine learning techniques for intelligent collocation point selection could yield significant improvements in computational efficiency. Lastly, parallelization and high-performance computing implementations should be explored to scale the method for large-scale scientific and engineering applications.

Acknowledgments: Authors are thankful to Prince Sultan University for APC and support through TAS research lab.
Funding information: This research was supported for APC by Prince Sultan University.
Author contribution: E. Aourir and H. Laeli Dastjerdi prepared the initial draft and included methodology. M. Oudani included investigation and formal analysis. K. Shah revised and included the formal analysis, investigation. T.Abdeljawad edited the and finalized the last version.
Conflict of interest: The authors declare no conflict of interest to announce.
Informed consent: This is not applicable.
Authorization for the use of human subjects: This is not applicable.
Authorization for the use of experimental animals: This is not applicable.
Data availability statements: No data was used in this article.

References

1. Xu K, Chen L, Lopes AM, Wang M, Wu R, Zhu M. Fractional-order Zener model with temperature-order equivalence for viscoelastic dampers. Fractal Fract 2023;7:714.
2. Madani YA, Rabih MN, Alqarni FA, Ali Z, Aldwoah KA, Hleili M. Existence, uniqueness, and stability of a nonlinear tripled fractional order differential system. Fractal Fract 2024; 8:416.
3. ALI Z. Theoretical and computational study of fractional-order mathematical models for infectious diseases [Doctoral dissertation]. Kuala Lumpur: Monash University; 2023.
4. Ali Z, Rabiei F, Rashidi MM, Khodadadi T. A fractional-order mathematical model for COVID-19 outbreak with the effect of symptomatic and asymptomatic transmissions. Eur Phys J Plus 2022;137:395.
5. He JH. Some applications of nonlinear fractional differential equations and their approximations. Bull Sci Technol 1999;15:86—90.
6. Ahmad WM, El-Khazali R. Fractional-order dynamical models of love. Chaos Solitons Fractals 2007;33:1367—75.
7. Wang G, Pei K, Chen Y. Stability analysis of nonlinear Hadamard fractional differential system. J Franklin Inst 2019;356: 6538—46.
8. Zhang L, Hou W. Standing waves of nonlinear fractional p-Laplacian Schrödinger equation involving logarithmic nonlinearity. Appl Math Lett 2020;102:106149.
9. Buhmann M, Iserles A. Stability of the discretized pantograph differential equation. Math Comput 1993;60:575—89.
10. Brunner H. Recent advances in the numerical analysis of Volterra functional differential equations with variable delays. J Comput Appl Math 2009;228:524—37.
11. Behera S, Ray SS. An efficient numerical method based on Euler wavelets for solving fractional order pantograph Volterra delay-integro-differential equations. J Comput Appl Math 2022;406:113825.
12. Ahmad I, Amin R, Abdeljawad T, Shah K. A numerical method for fractional pantograph delay integro-differential equations on Haar wavelet. Int J Algorithm Comput Math 2021;7:28.
13. Yang Y, Huang Y. Spectral-collocation methods for fractional pantograph delay-integrodifferential equations. Adv Math Phys 2013;2013:821327—14.
14. Dehghan M, Shokri A. Numerical solution of the nonlinear Klein-Gordon equation using radial basis functions. J Comput Appl Math 2009;230:400—10.
15. Laeli Dastjerdi H, Nili Ahmadabadi M. Moving least squares collocation method for Volterra integral equations with proportional delay. Int J Comput Math 2017;94:2335—47.
16. Hosseinian A, Assari P, Dehghan M. The numerical solution of nonlinear delay Volterra integral equations using the thin plate spline collocation method with error analysis. Comput Appl Math 2023;42:83.
17. Aourir E, Izem N, Dastjerdi HL. A computational approach for solving third kind VIEs by collocation method based on radial basis functions. J Comput Appl Math 2024;440:115636.
18. Aourir E, Izem N, Dastjerdi HL. Numerical solutions of a class of linear and nonlinear Volterra integral equations of the third kind using collocation method based on radial basis functions. Comput Appl Math 2024;43:117.
19. Dehghan M, Salehi R. The numerical solution of the non-linear integro-differential equations based on the meshless method. J Comput Appl Math 2012;236:2367—77.
20. Aljawi S, Aljohani S, Kamran AA, Mlaiki N. Numerical solution of the linear fractional delay differential equation using Gauss-Hermite quadrature. Symmetry 2024;16:721.
21. Franke R. Scattered data interpolation: tests of some methods. Math Comput 1982;38:181—200.
22. Bibi M, Arif MS, Nawaz Y, Kerdid N. Numerical analysis of heat and mass transfer in tangent hyperbolic fluids using a two-stage exponential integrator with compact spatial discretization. Comput Model Eng Sci (CMES) 2025;145:p537—569.
23. Aljawi S, Aloqaily A, Mlaiki N. A local meshless method for the numerical solution of multi-term time-fractional generalized Oldroyd-B fluid model. Heliyon 2024;10.
24. Wendland H. Scattered data approximation. Cambridge: Cambridge University Press; 2005.
25. Fasshauer GE. Newton iteration with multiquadrics for the solution of nonlinear PDEs. Comput Math Appl 2002;43:423—38.
26. Cheng AD, Golberg MA, Kansa EJ, Zammito G. Exponential convergence and H-C multiquadric collocation method for partial differential equations. Numerical Methods for Partial Differential Equations. Int J 2003;19:571—94.
27. Fasshauer GE, Zhang JG. On choosing “optimal” shape parameters for RBF approximation. Numer Algorithms 2007;45:345—68.
28. Pozrikidis C. The numerical solution of integral equations of the second kind. By KE Atkinson. Cambridge: Cambridge University Press; 1997:552—p.
29. Gripenberg G, Londen SO, Staffans O. Volterra integral and functional equations. Cambridge University Press; 2004.
30. Atkinson K, Flores J. The discrete collocation method for nonlinear integral equations. IMA J Numer Anal 1993;13:195—213.
31. Fang W, Wang Y, Xu Y. An implementation of fast wavelet Galerkin methods for integral equations of the second kind. J Sci Comput 2004;20:277—302.
32. Vainikko G. First kind cordial Volterra integral equations 2. Numer Funct Anal Optim 2014;35:1607—37.
33. Mirzaei D, Dehghan M. A meshless based method for solution of integral equations. Appl Numer Math 2010;60:245—62.
34. Jafari H, Tuan NA, Ganji RM. A new numerical scheme for solving pantograph type nonlinear fractional integro-differential equations. J King Saud Univ Sci 2021;33:101185.
35. Zhao J, Cao Y, Xu Y. Sinc numerical solution for pantograph Volterra delay-integro-differential equation. Int J Comput Math 2017;94:853—65.
36. Ezz-Eldien SS, Doha EH. Fast and precise spectral method for solving pantograph type Volterra integro-differential equations. Numer Algorithms 2019;81:57—77.
37. Rezabeyk S, Abbasbandy S, Shivanian E. Solving fractional-order delay integro-differential equations using operational matrix based on fractional-order Euler polynomials. Math Sci 2020;14:97—107.